Institute of Space and Aeronautical Science, University of Tokyo
Report No. 563, August 1978

Diagnostic Studies of SEPAC Test in NASDA Space Chamber

By

Tatsuzo OBAYASHI, Kyoichi KURIKI, Nobuki KAWASHIMA,
Makoto NAGATOMO, Isao KUDO*, Keiken NINOMIYA
Akio USHIROKAWA, Masaki EJIRI and Susumu SASAKI

Abstract: Beam, plasma and waves induced by their interactions were studied in NASDA Large Space Chamber. EBA (Electron Beam Accelerator) and MPD (Magnetoplasma-dynamic) arcjet, which generate the beam and plasma, were SEPAC (Space Experiment with Particle Accelerators) Engineering Models. Diagnostic probes used were also EM's. Nude ionization gauge monitored background pressure being unaffected by EBA and MPD operations. A retarding potential analyzer at the ground potential collected currents of various polarities depending on the type of accelerator. Some results exhibited oscillatory behavior. A photometer and a TV camera monitored the radiation from MPD and beam generated plasmas. A floating potential probe provided the data of charge neutralization. Beam-generated waves were monitored by antennas.

Contents

* Electrotechnical Laboratory

1. Introduction

The laboratory experiment for simulating a SEPAC system aboard a first spacelab was carried out in a large vacuum space chamber at NASDA. Though this campaign was mainly devoted to the tests of the guns, various kinds of measurements to

NASDA EXPERIMENT DG BLOCK DIAGRAM

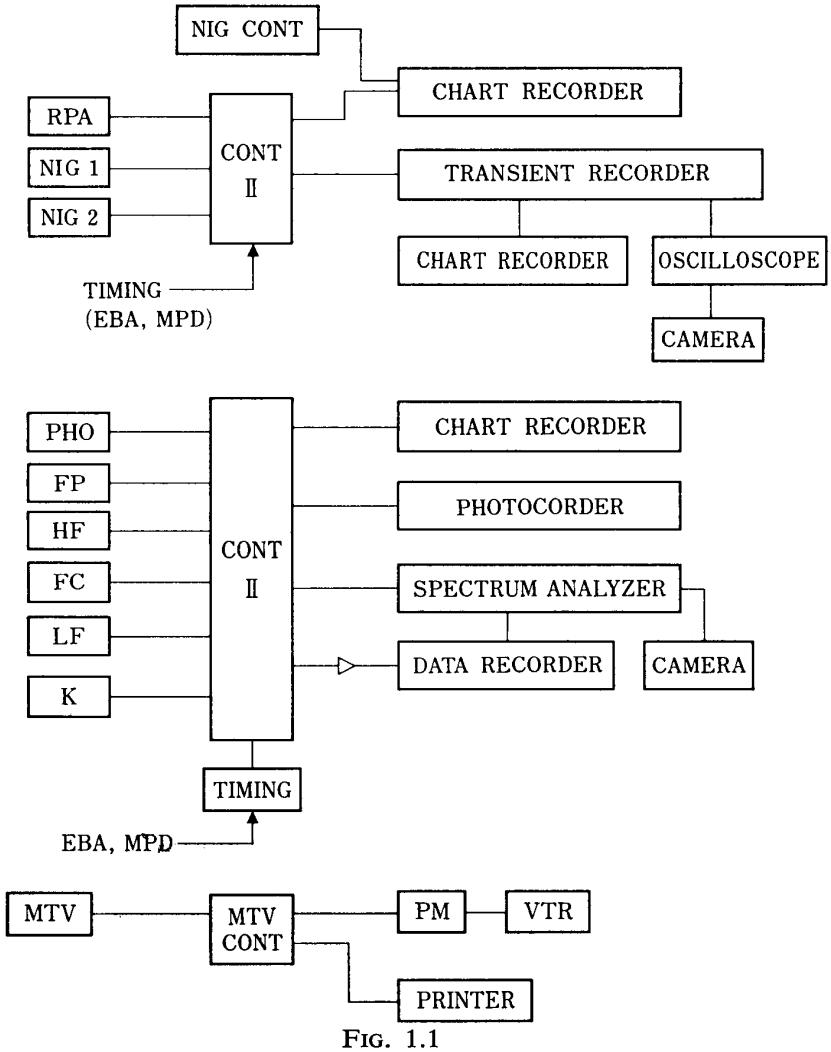

Fig. 1.1

study characteristics and their interactions of electron beam, plasma beam and neutral gas plume were carried out by using following diagnostic instruments; an electron current collector (RPA), two nude gauge vacuum sensors (NIG1 and 2), a photo-meter (PHO), a floating probe (FP), a high-frequency wave detector (HF), Faraday Cup (FC), a low-frequency wave detector (LF), a K-vector (K) and a monitor television camera (MTV).

The system block-diagram is illustrated in Fig. 1.1, and the layout in Fig. 1.2. (1) MTV is a SIT tube TV camera which monitors the beam path in space. Note that the time resolution of this measurement is about 30 ms. (2) RPA measures an electron current to the collector which is located in the down stream of the beams. (3) NIG detects a neutral gas pressure with a time resolution of 1 ms., NGP propagation profile being measured. (4) PHO has three filters of 3914 Å, 5577 Å and 6300 Å and measured $N^+$and 0^+ excitations by beams. (5) FP detects a floating potential of the electron gun refered to the space potential, three separate electrodes being used. (6) LF, HF, FC and K are used for detections of electro-magnetic and/or electro-static waves excited by the beams.

Following sections depict an indivisual measurement result. Though all of obtained results have not been fully understood, the detail designs of DG components were based upon this experiment, in a sense that resolution, sensitivity, dynamic range, operational sequences, etc. are concerned.

2. NIG Test

2.1 *General*

NIG is a Nude-gauge-type Ionization Gauge which measures an environmental neutral gas pressure (N_2 equivalent) with a time response of about 1 msec and an

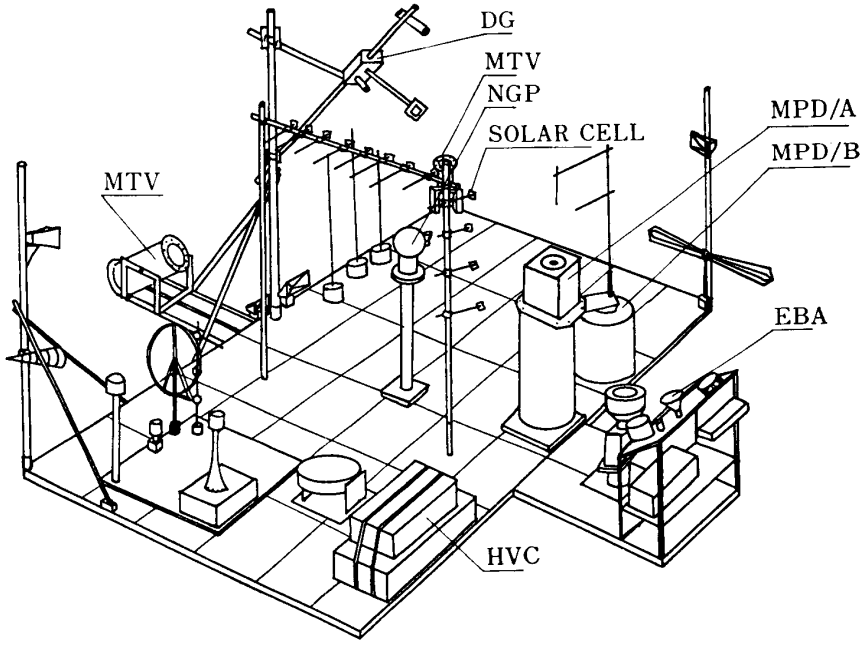

Fig. 1.2

accuracy less ahan 20%. In this experiment two gauges were used and located at the middle port of a pole (NIG 1) and its foot (NIG 2), respectively. It should be noted that the fight-type gauge under development for SEPAC is not identical with the used one but based upon this type.

2.2 *NIG System*

Fig. 2.1 illustrates one of NIGs located at the middle port of the pole. To avoid the light from the filament disturbing a light emission excited by a beam, the cylindrical shielding covered the sensor head. The temperature monitor sensor was placed on the basement of the gause. The controller to supply an electrical power and to measure a collector current was settled outside of the vacuum chamber. Since the interconnecting cables between the sensor head and the controller was too long to neglect its effect, the calibration had been done prior to the installation in the chamber.

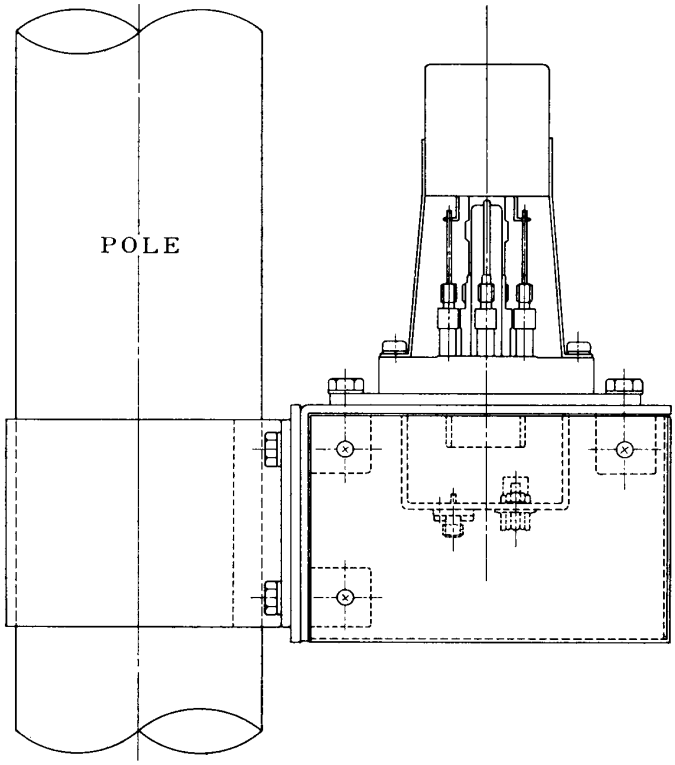

FIG. 2.1. Nude Ionization Gauge

2.3 *Experimental Results*

Malfunction of NIG in the first day of the vacuum pumping with cooling shrouds came from the facts that the sensor head was very severely cooled to less than $-100°C$ where a filament was not heated enough to give a proper emission current and that, due to the line drop of the filament voltage, a power to the filament was unusually small. The temperature was, however, once raised to the normal operational value after a day, NIG gave correct pressure data as discussed below.

Typical examples are shown in Fig. 2.2 (a), (b) and (c) corresponding to the

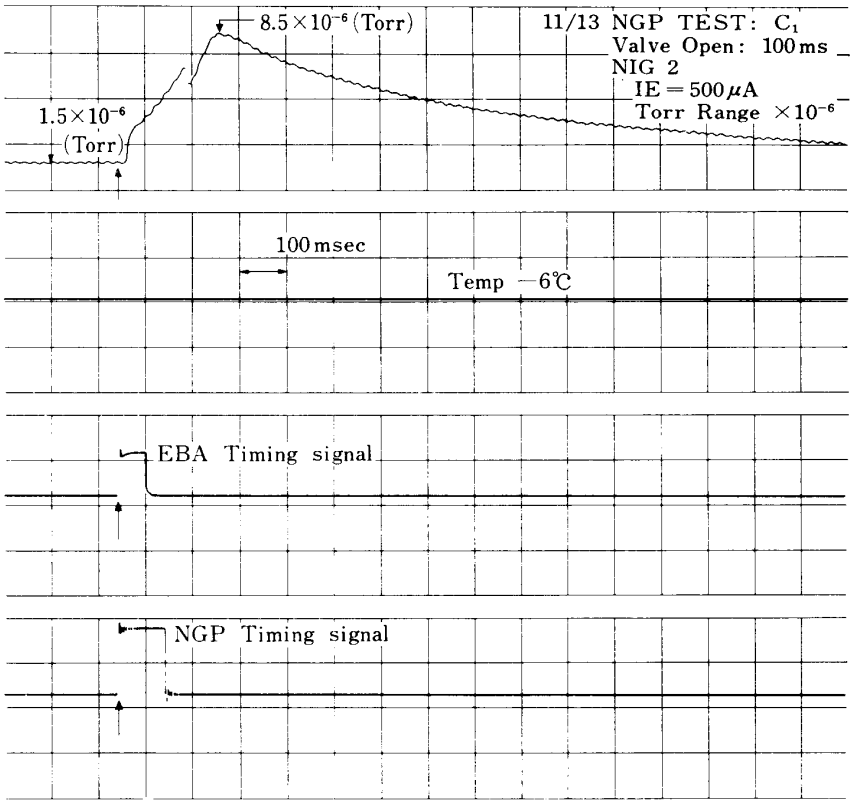

FIG. 2.2 (a). NIG 2 Record associated with NGP TEST C_1

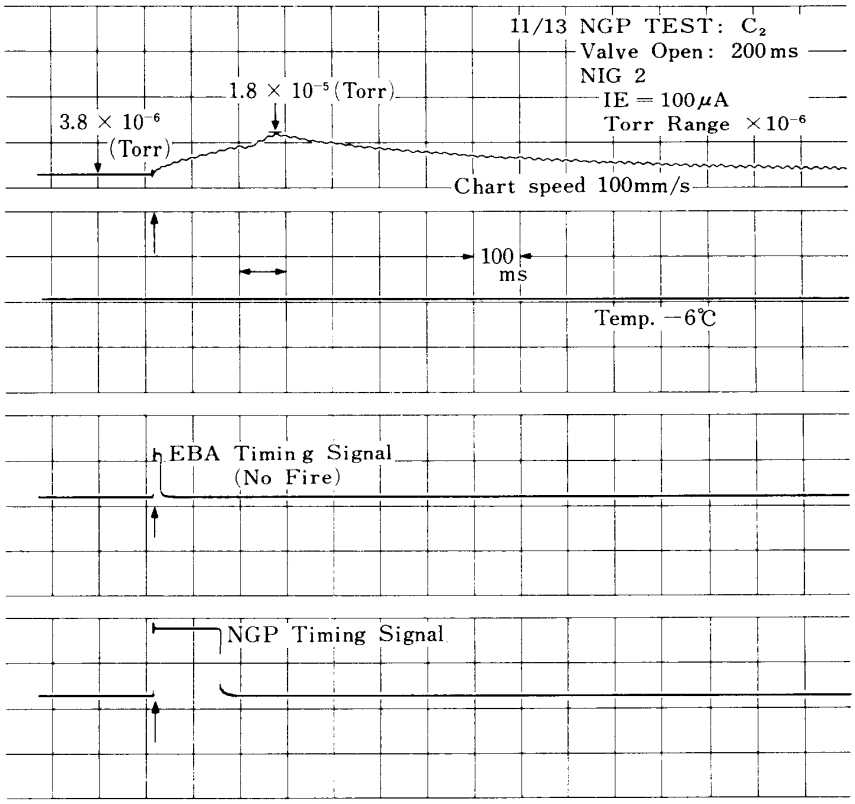

FIG. 2.2 (b). NIG 2 Record associated with NGP TEST C_2

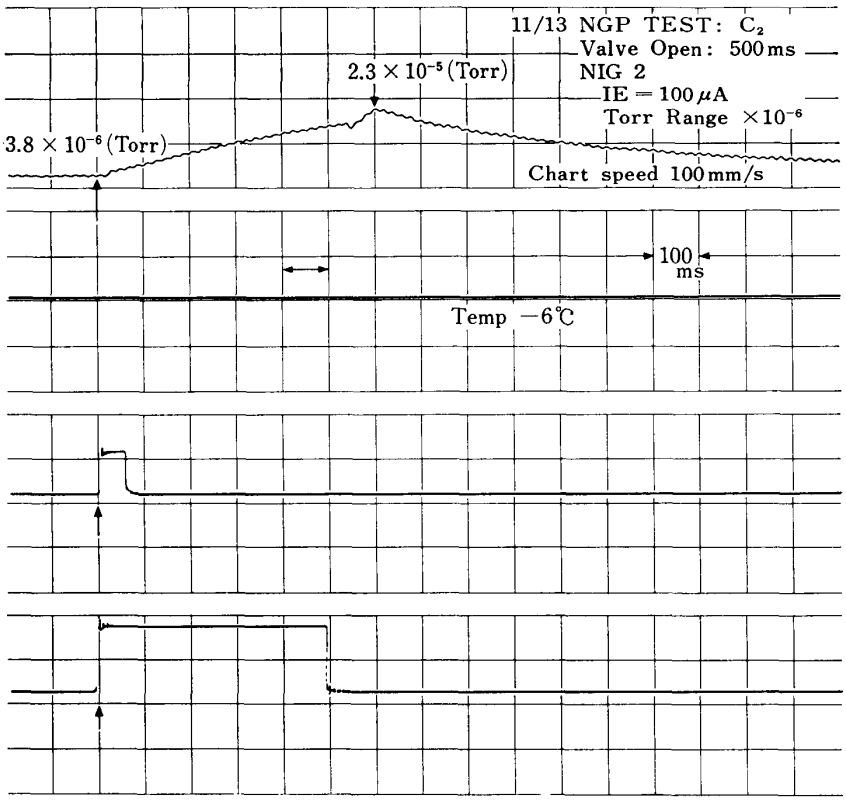

FIG. 2.2 (c). NIG 2 Record associated with NGP TEST C_5

NGP conditions of EJNT=0.1 sec, 0.2 sec and 0.5 sec with a constant EJNP= 3.6 AT; maximum pressures measured by NIG 2 are 8.5×10^{-6}, 1.8×10^{-5}, and 2.3×10^{-5} Torr, with different relative time delays corresponding to each condition. All of these examples are simultaneous EBA/NGP operation (in the case of (b) EBA did not fire) but the effect of EBA fire on neutral pressure was very small though a slight enhancement was observed due to the outgassing by the return current of EBA. As for the MPD operation, the change in pressure was also negligible.

2.4 *Conclusion*

In a large vacuum chamber at NASDA, EBA and MPD firings did not disturb a neutral pressure so that we can simulate a space environment in an ionoshperic region. The change in pressure due to NGP operation is clearly monitored by NIG with a sufficient time resolution. The basic data desing of a fiighttype ionization gauge and its onboard controller are obtained in this experiment.

3. RPA TEST

3.1 *General*

RPA is an electron/ion collector with a floating bias voltage i.e. no external applied voltage, its potential being idential to the ground potential of the system. Note that in this experiment, there were two seperate groundings; one was for

EBA, MPD and a part of DG equipments and called as a floating ground, and the other was a space chamber grounding connected to the earth and called as a chamber ground. Both NIG in sec. 2 and RPA had a chamber ground, and the other DG equipments had a floating ground. If two ground systems are absolutely separated in a sense of DC and/or AC, there should not be any currents to the RPA from EBA and/or MPD beam emissions. But it was anticipated that the emitted beams would bridge electrically two ground systems by produced plasma clouds, and that if once there emerged an electrical potential relation between two, RPA could measure the currents. These currents give direct information about the instabilities produced in a beam stream if any. Since the position of RPA sensor was unfortunately fixed, beam propagating profiles were not measured.

3.2 *RPA System*

RPA was located at the top of the DG pole, the sensor being directed towards EBA gun direction which was along the geomagnetic field in the chamber. Fig. 3.1 illustrates the RPA sensor: the aperture is 30 mm in diameter i.e. about 7 cm^2. Inside the sensor, the pre-amplifier was installed, together with an electrical heater and a temperature sensor in order to maintain an environmental temperature

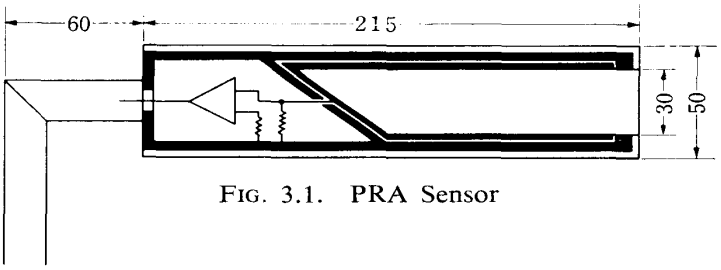

FIG. 3.1. PRA Sensor

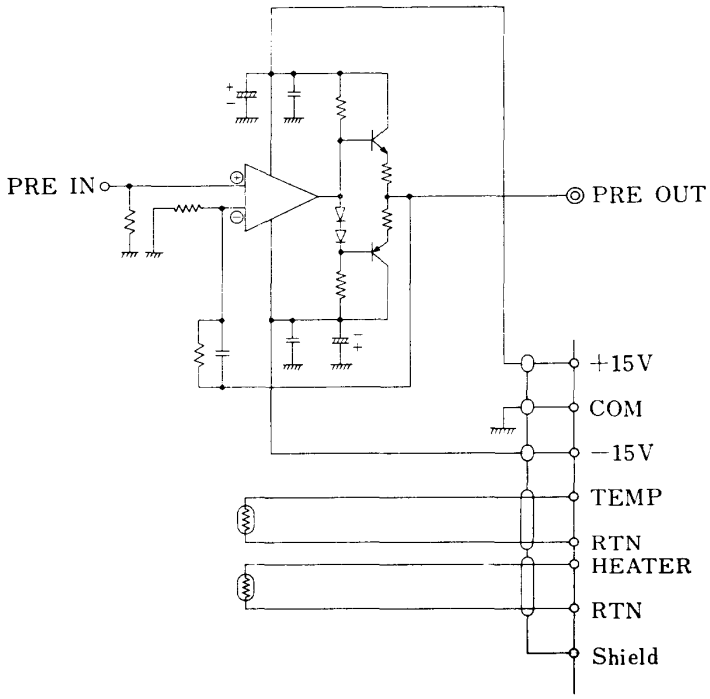

FIG. 3.2. RPA PRE-AMP

around the pre-amplifier to be above 0°C. The circuit is shown in Fig. 3.2 with its input-output characteristics being 3×10^4 V/A. The experimental results are presented in a form of output voltage as a function of time from which the input current density is easily obtained using above relation and area of RPA aperture. Two recording systems were used: One was a trasient recorder which sampled 250 data points at a specified sampling rate and its outputs were recorded in a chart recorder, and the other was a memoryscope (oscilloscope with a capability of memory) and data were taken by a polaroid camera.

3.3 *Experimental Results*

The experiments were carried out with MPD mode, EBA mode, EBA/NGP and EBA/NGP modes. The experimental conditions are parameterized as shown in Appendix. Typical examples are illustrated in the following Figs. 3.3.

(1) MPD firing test

This test was conducted with various MPD firing conditions and with the earth mode operation i.e. two grounding systems are bounded together. The trigger pulse of MPD FAVSCR was used to start a sampling of the transient recorder, about 1.2 msec from which MPD firing was started. The results were illustrated in Figs. 3.3 (a, b). In most of the MPD firing mode A, RPA measured an electron current to the collector with large amplitude oscillations of several hundred Hz. Total current decreases with decrease of CHGV 1. But in B mode, RPA picked up an ion current; opposite to the case of A mode. Current profile with time is also changed. Peak ion current decreased with decrease of CHGV 1. This difference in current between A and B modes are not understandable in the current design status of two MPD-AJ instruments, but the small difference in plasma discharge may produce a different space potential with respect to the ground potential of the RPA. The oscilatory behaviours of current have not been identified yet; whether it comes from the plasma instabilities or the potential change of plasma due to the finite wall effects, or else.

To compare the current from the EBA firing the observed current density of MPD, either electron or ion, is about 2 order of magnitude larger than that of the EBA, as is examined in the subsequent sections.

(2) EBA firing test

This firing test was also an earth mode operation and concucted by changing an acceleration voltage (V), heater current (I_H), beam emission current (I_B), and emission duration time (τ) which are indicated in Appendix. The typical recorded examples are shown in Figs. 3.4 (a–d). It is natural that RPA detects an electron current during the EBA beam emission but the current density is not proportional to the beam current at the electron gun.

There are three kinds of electron current profile with change in an accelerating voltage, those are (1) at lower voltage there is no evident oscillation with time though the current intensity, strictly speaking, is not constant, (2) when the voltage increases to about 2 kV there emerges a low-frequency large amplitude oscillation

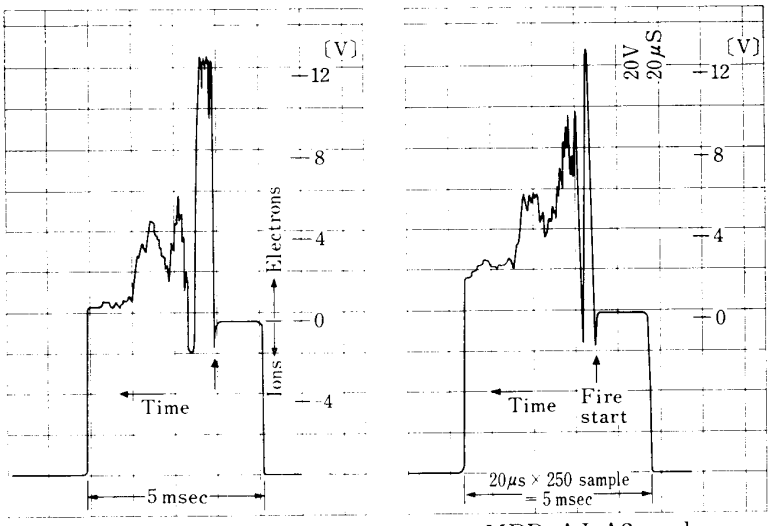

MPD-AJ A1 mode　　MPD-AJ A2 mode

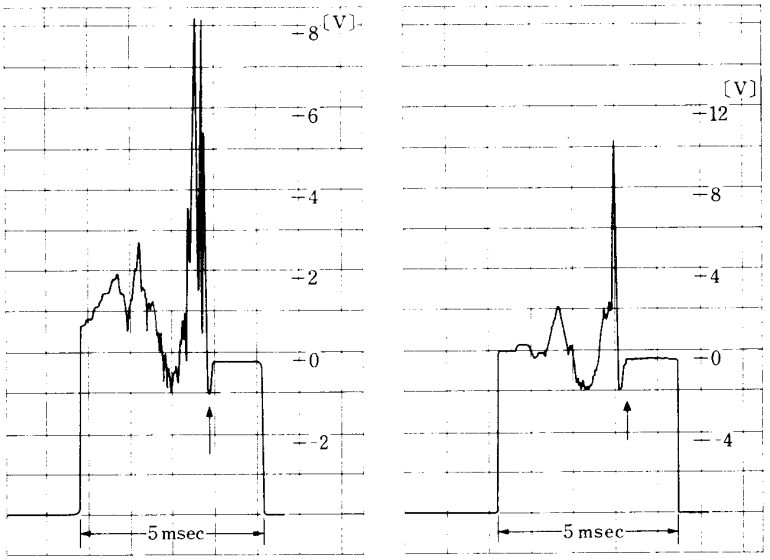

MPD-AJ A3 mode　　MPD-AJ A4 mode

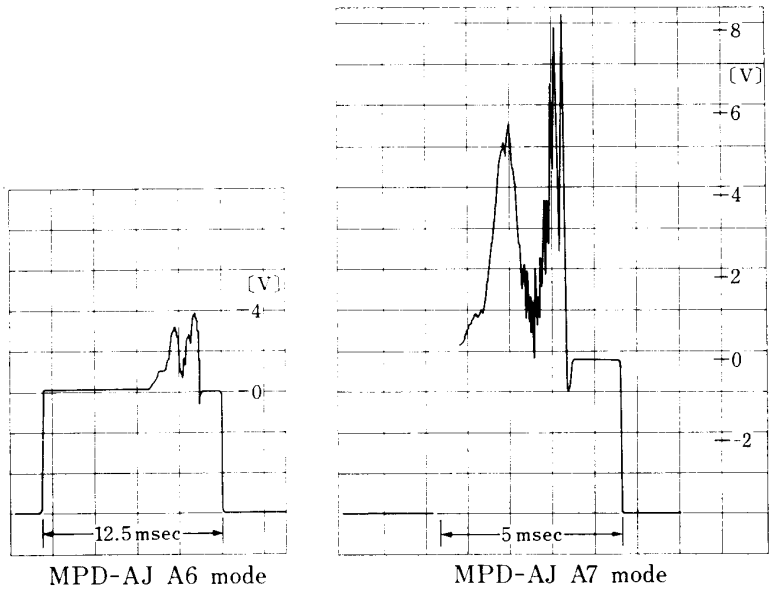

MPD-AJ A6 mode　　MPD-AJ A7 mode

FIG. 3.3 (a). PRA data for MPD/A

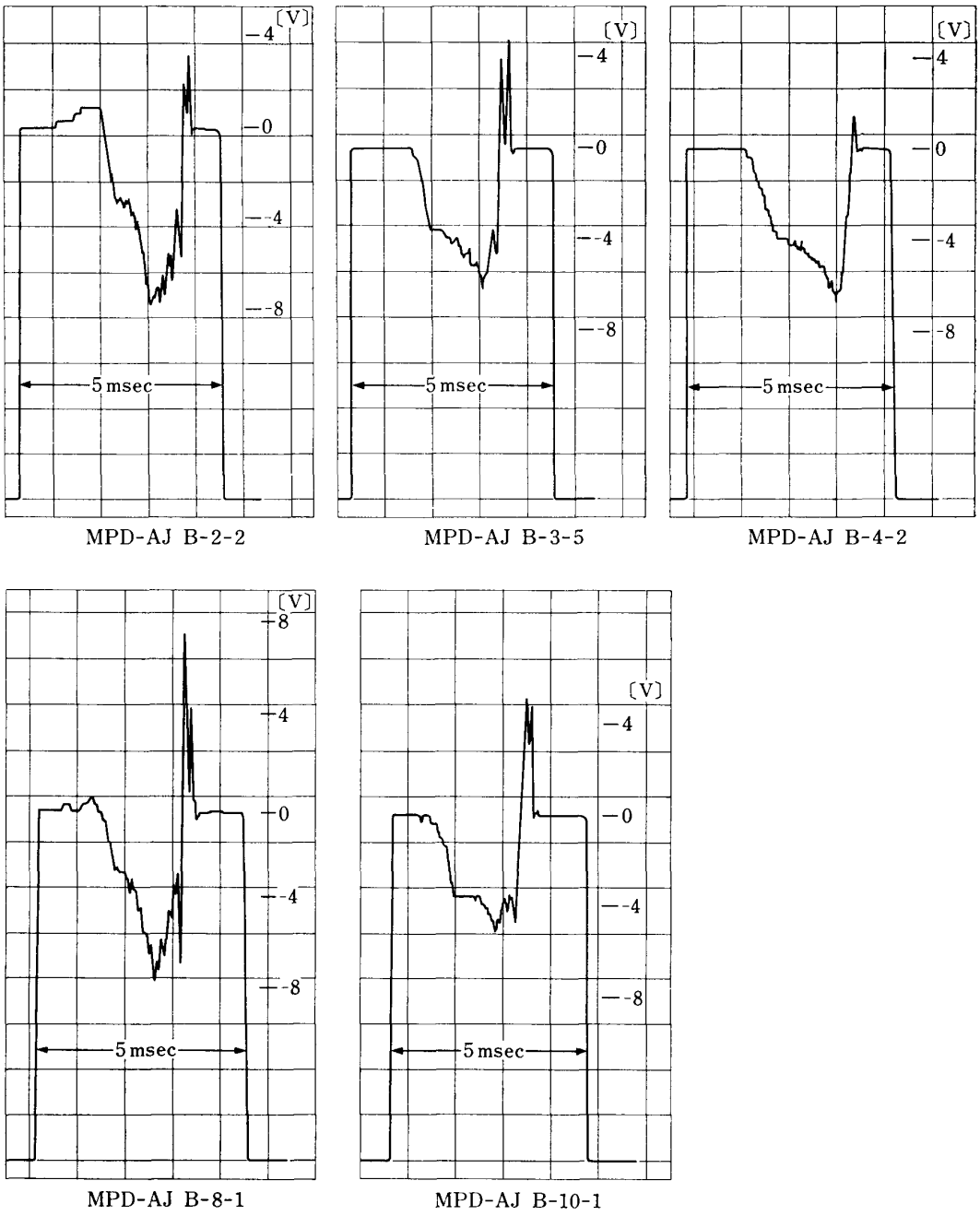

FIG. 3.3 (b). RPA data for MPD/B

with around 50 Hz, and (3) above 3 kV the current shows a high frequency fluctuation around kHz. There is no explanation for these results at the present but there may be some mode changes in beam instabilities. When the beam current increases (Fig. 3.4(c)), the high-frequency fluctuation disappeares and large-amplitude oscillation with less than 50 Hz is observed again.

The typical high-frequency fluctuation in electron current is depicted in Fig. 3.4(d) where EBA was fired together with a neutral gas plume simultaneously ejected from the NGP. The experiment parameters are: $V=7.5$ kV, maximum perviance with $\tau=50$ msec and C_1 mode of NGP. An average current density is

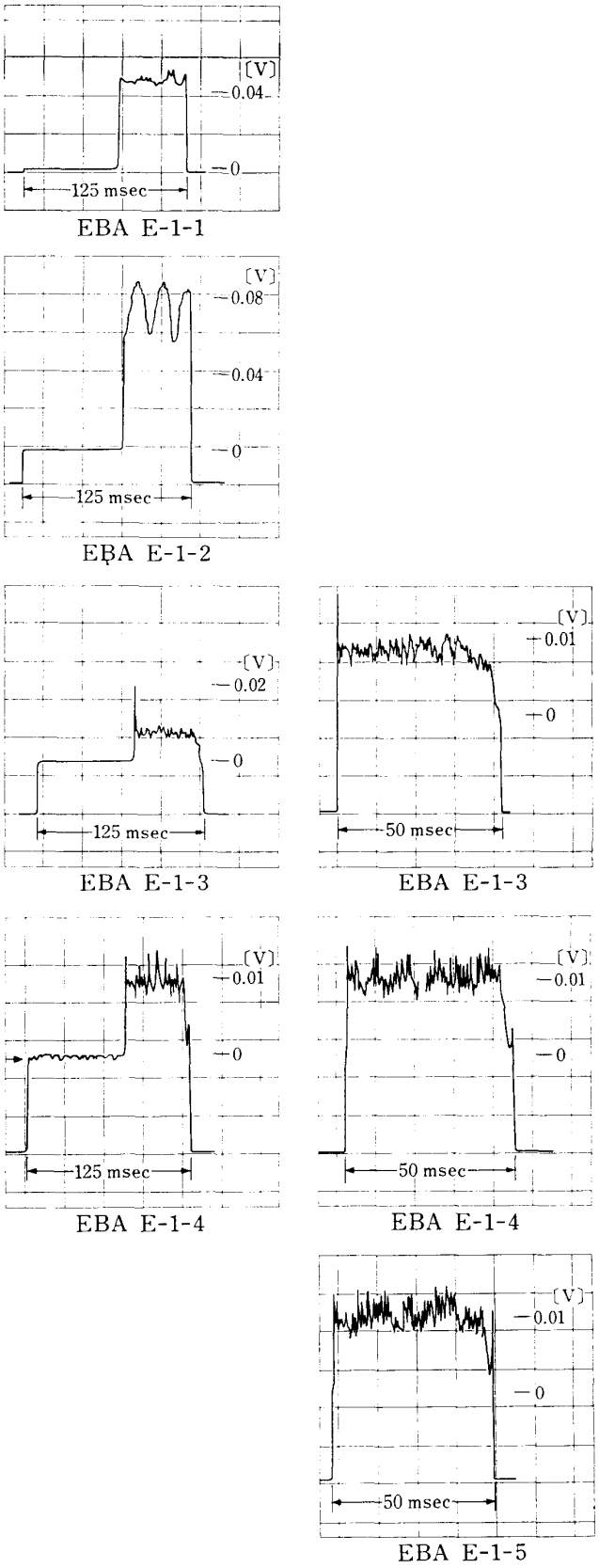

FIG. 3.4 (a). PRA data for EBA E-1

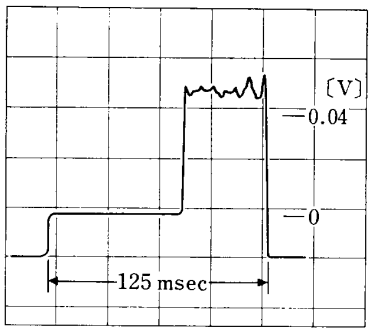

EBA E-2-1

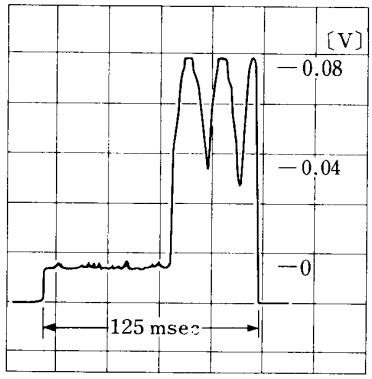

EBA E-2-2

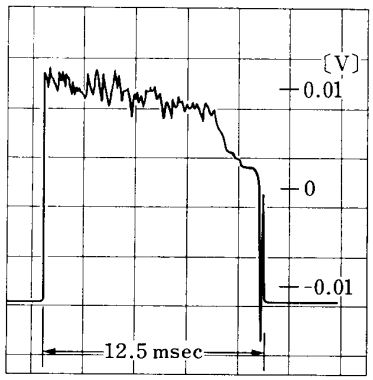

EBA E-2-3

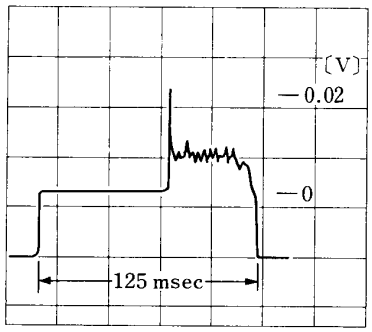

EBA E-2-3

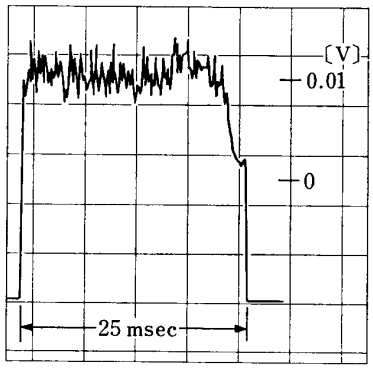

EBA E-2-4

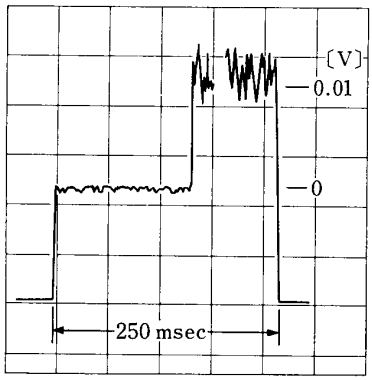

EBA E-2-5

FIG. 3.4 (b). RPA data for EBA E-2

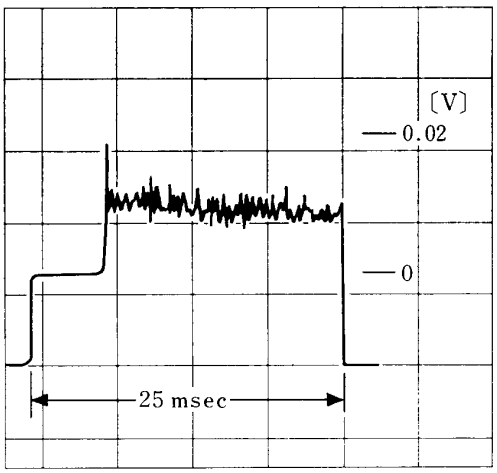

EBA E-3-3a

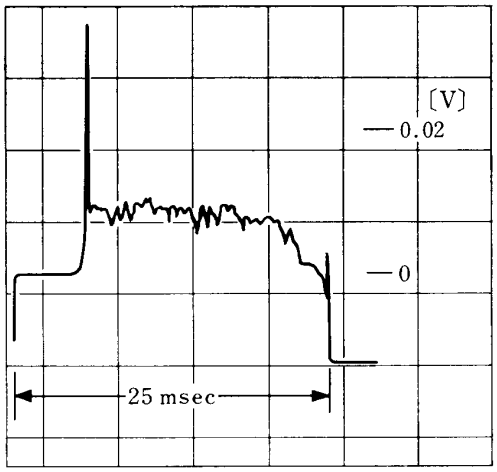

EBA E-3-3b

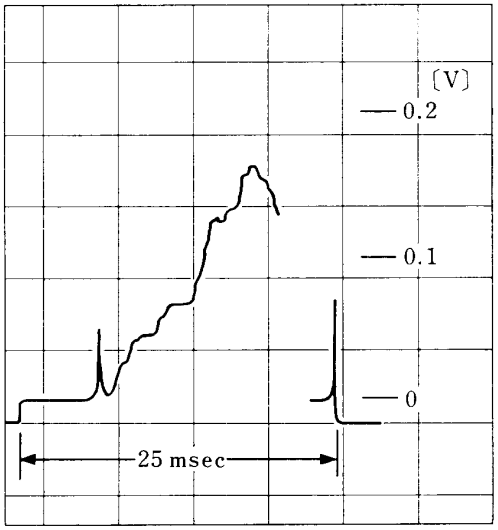

EBA E-3-3c

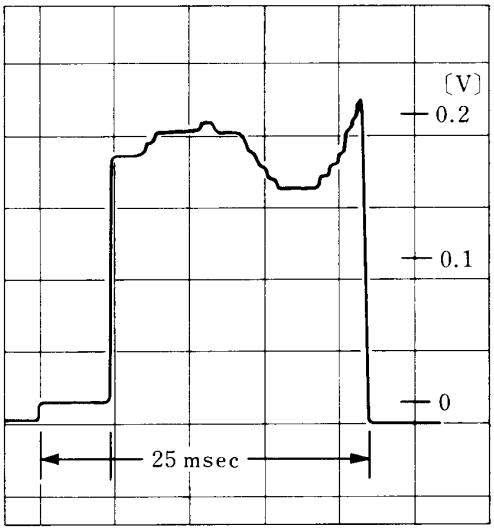

EBA E-3-3d

FIG. 3.4 (c). RPA data for EBA E-3-3a to 3d.

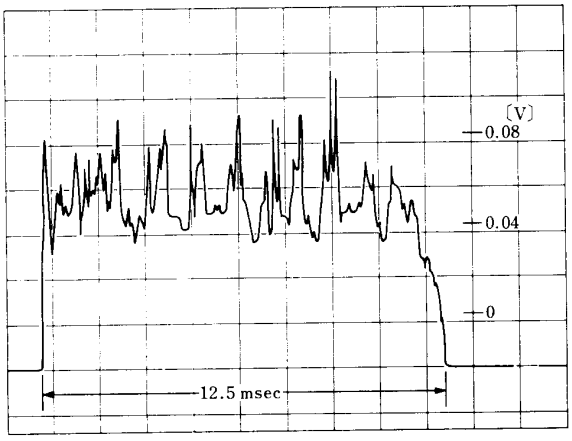

EBA/NGP RUN-3-1

FIG. 3.4 (d). RPA data showing a fine structure of current oscillation due to EBA firing (details in the test).

about 0.2 μA/cm^2. These data will be compared with a theoretical simulation experiment being under development, and might be analysed in a form of frequency spectrum.

(3) EBA/MPD simulteneous operations

To investigate an effect of MPD firing to EBA operation, MPD was fired during an EBA beam emission with both accelerations' grounding being a floating mode i.e. separated from the chamber ground. Though there were several modes where the delay time of EBA/MPD firings were changed, Fig. 3.5 indicates one example of timing pulse diagram which corresponds to the following results in Fig. 3.6. EBA trigger pulse and MPD trigger pulse were used as a trigger of the oscilloscope to memorize a wave form of beam current. All examples are taken with EBA trigger pulse unless otherwise mentioned in the figures, that means EBA beam current is observed from the left end of the screen and MPD FAVSCR is activated approximately 3 msec delayed, companied with MPD firing 1.2 msec ($A_1 \sim A_7$ modes) or 0.8 msec ($B_1 \sim B_7$ modes) delayed.

As has been examined previously, the current to RPA associated with EBA firing is very small compared with that for MPD firing, it is very difficult to see the current change in EBA beam due to MPD firing during which the current of MPD is dominant. The current due to the MPD operation, however, demonstrates much different features from that for MPD single firing without EBA firing, and the oscillatory current profile depends on the EBA beam emission current as shown in Fig. 3.6 (c and d), E–9–1$\sim$6 modes where I_B increases from 3 to 400 mA with a constant V=5 kV. The change of current profile due to MPD mode changes (A_2, A_3, B_1, B_3) are illustrated in Fig. 3.6 (e and f). Detail examinations have not finished, but the coupling of two beams however are clearly observed. Note that in order to interprete these experimental results the potential change between two grounding systems must be taken into account; those informations are available from the PLP-FP experiment. PHO also gives informations of current density of each beam and their interactive changes.

(4) EBA single emission with a floating grounding

The FP as will discussed in next section and other instruments which measured a potential difference between two grounding systems proved that the EBA floating ground with respect to the chamber ground becomes a positive voltage whose value is approximately equal to the beam voltage when there is no charge neutralization by MPD and/or NGP operations. Therefore the RPA is negative with respect to EBA beam potential and measures a positive ion during a beam emission of EBA. This is clearly observed in the result illustrated in the top panel of Fig. 3.7(a). It shows very curious profile with time though a current density of ion is same order of magiitude of that of electron observed in the earth mode operation. The potential profile did not show this kind of fluctuation.

(5) EBA/NGP simulteneous operations

Since NGP ejects a large amount of neutral gas (N_2) which is ionized by the

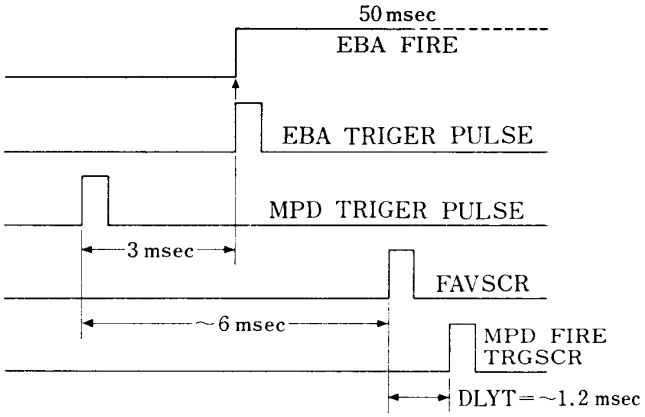

TIMING RELATIONS OF EBA AND MPD FIRINGS

FIG. 3.5. Timing pulses diagram for EBA/MPD simultaneous emissions experiment.

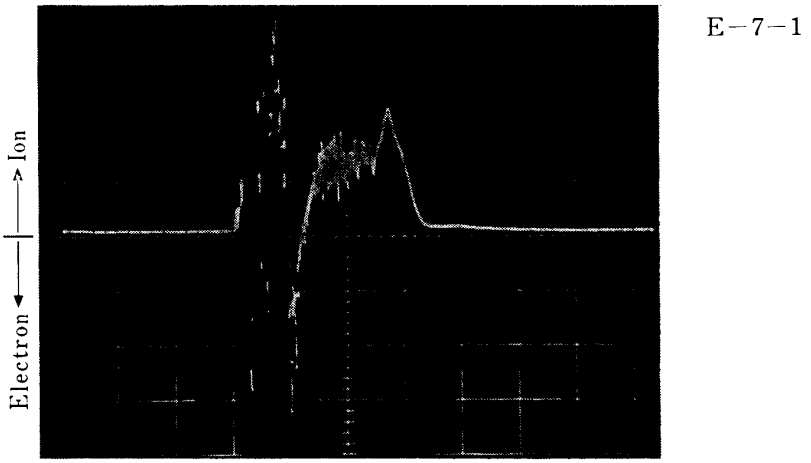

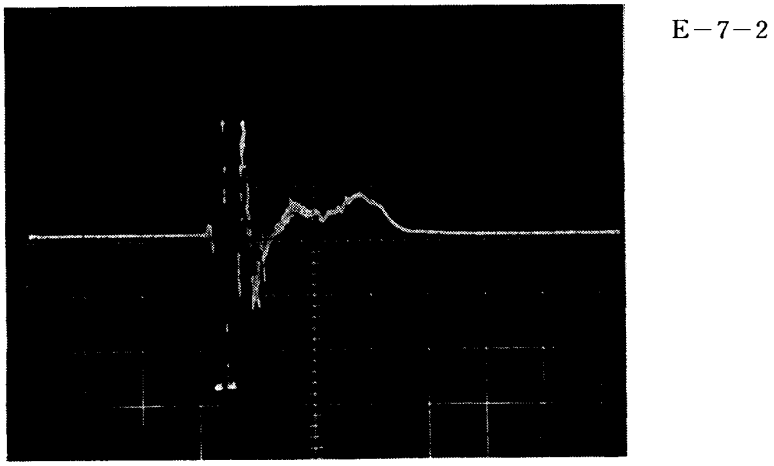

FIG. 3.6 (a). RPA data for EBA/MPD experiment (V: 5 V/Div. and H: 1 msec/Div.).

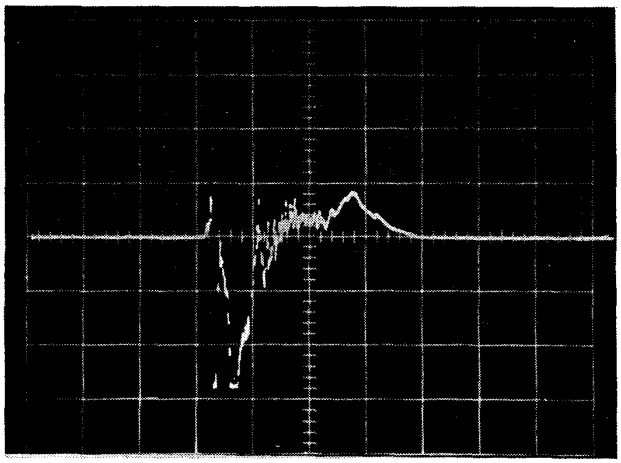

E−8−1

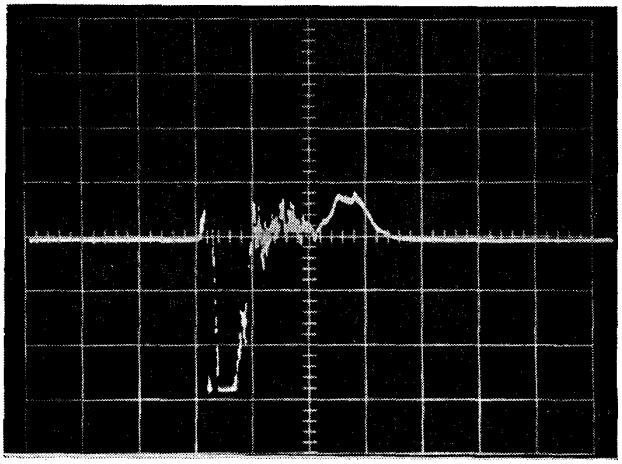

E−8−2

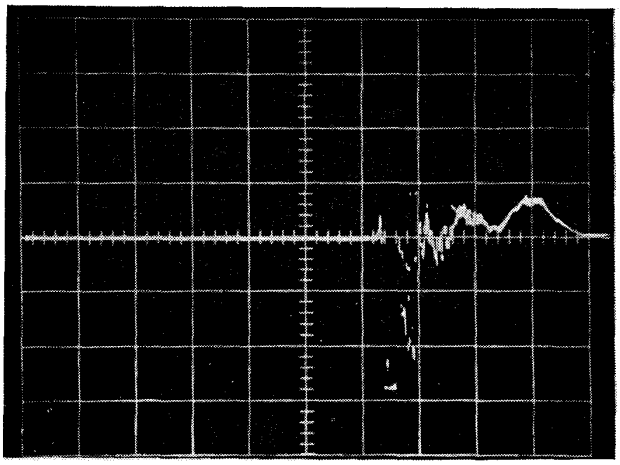

E−8−2
MPD only
without EBA fire.
MPD trigger pulse.
E−14−3a

FIG. 3.6 (b). RPA data for EBA/MPD experiment (V: 5 V/Div and H: 1 msec/Div.).

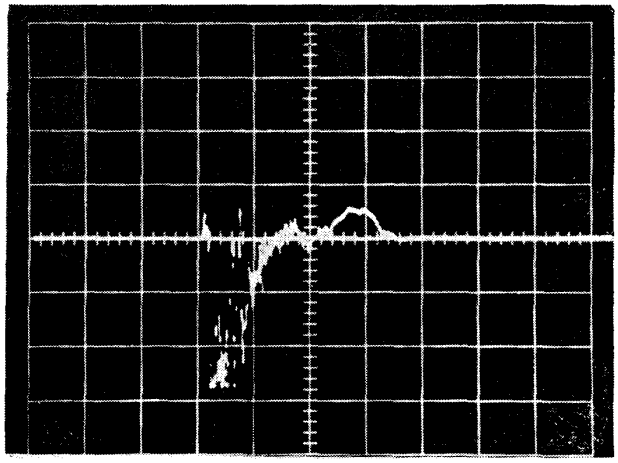

E−9−1

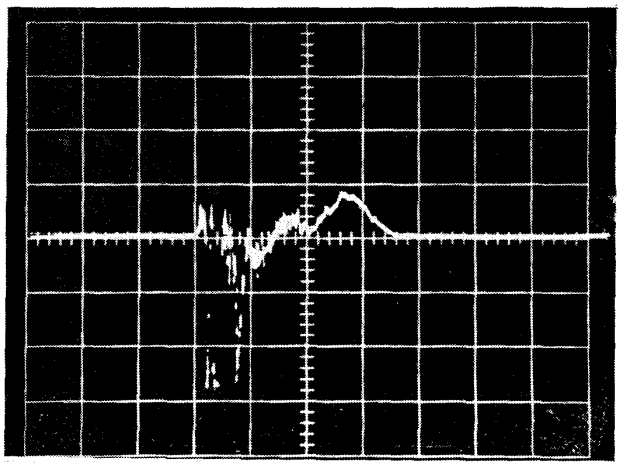

E−9−2

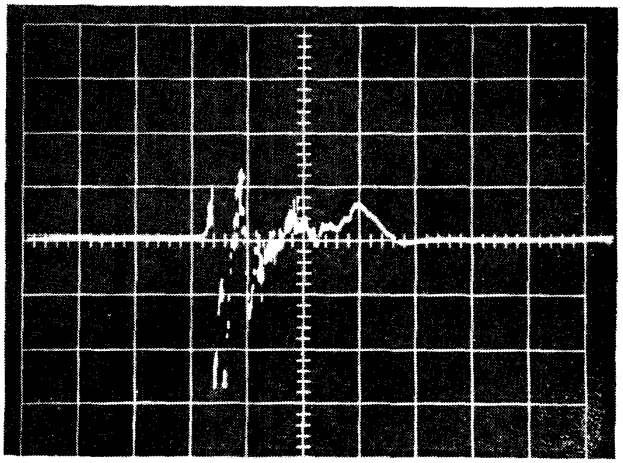

E−9−3

FIG. 3.6 (c). RPA data for EBA/MPD experiment (V: 5V/Div. and H: 1 msec/Div.).

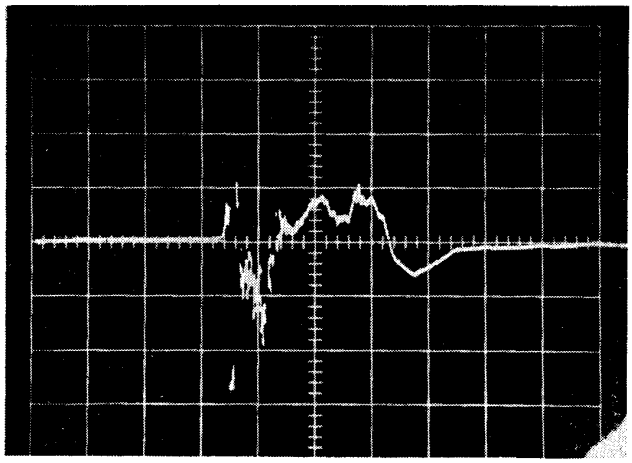

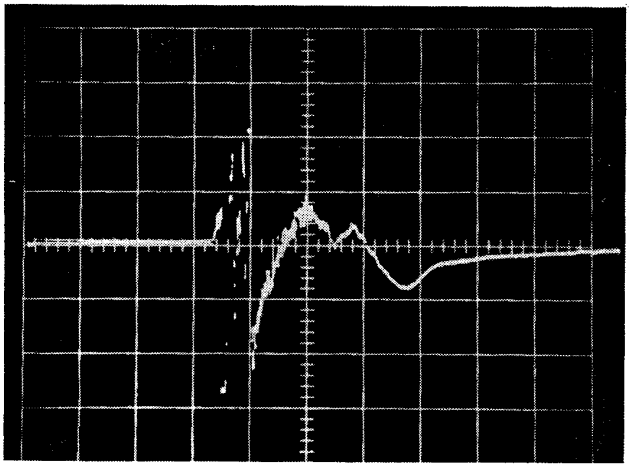

FIG. 3.6 (d). RPA data for EBA/MPD experiment (V: 5V/Div. and H: 1 msec/Div.).

energetic electrons from EBA, two ground systems are bridged electrically by the produced plasma cloud. Therefore the RPA detects an electron current. These effect of NGP operation to the beam current was examined and the results are shown in Fig. 3.7 (a–c) with various change of time delay (τ_{NE}) of NGP ejection with respect to EBA emission. In the simultaneous operation i.e. $\tau_{NE}=0$, a positive ion current is flown to the RPA in the beginning of the emission and later the current changes its polarity. In the case of $\tau_{NE}=1.5$ sec, the effect of NGP is still existing such that RPA data presents a high-frequency fluctuation of an electron current like that observed in EBA earthmode operation.

3.4 *Conclusion*

Experiments under various kinds of operational modes of EBA, MPD, EBA/MPD, EBA/NGP and different grounding modes were performed in order to examine the current density to the RPA collector. Several different current profiles, electron and ion, were observed and classified according to the different experiment parameters. Some of the results especially the current polarities can be reasonably

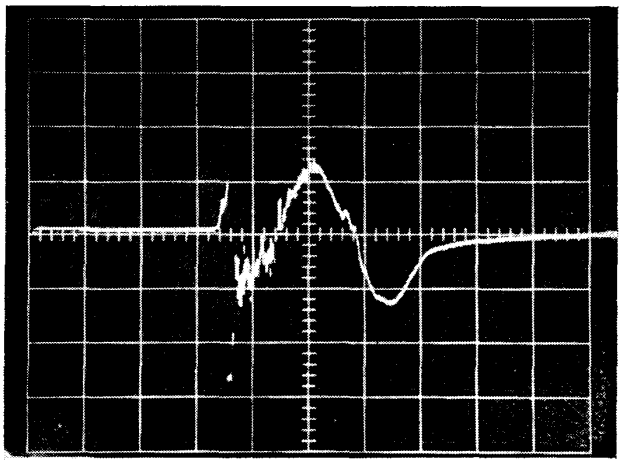

E−10−2

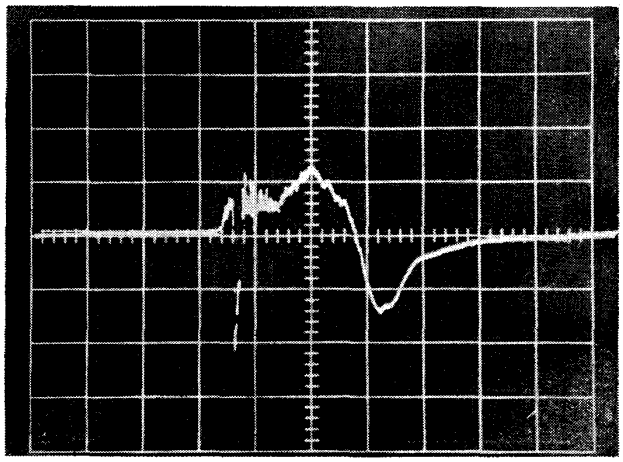

E−10−3

FIG. 3.6 (e). RPA data for EBA/MPD experiment (V: 5V/Div. and H: 1 msec/Div.).

explained but their oscillatory behaviors have not been understood theoretically yet. Comparison with the data from PHO, PLP-FP and PWP and other instruments are also needed for the further analysis of these data.

4. PHO TEST

4.1 *General*

PHO monitors the irradiance in the visible region due to interactions of electron beams from EBA and plasma beams of MPD with a neutral gas, and also measures a back-ground natural irradiance of atmosphere. PHO used in this experiment is an engineering type for SEPAC/PHO with three kinds of filters in order to observe and identify a specific wave length corresponding to each excitation mechanism; 3914 Å for N_2^+, 5577 Å and 6300 Å for O^+. This test also included the system test of this engineering model such that the thermo-vacuum test to check a motor drive mechanism for 2-axis gimbal system, filter exchange, iris control systems, etc. As for the mechanical structure, MTV in sec. 7 is

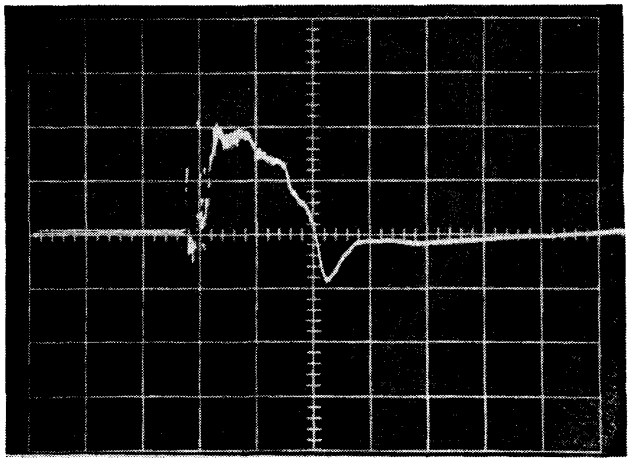

E−10−5

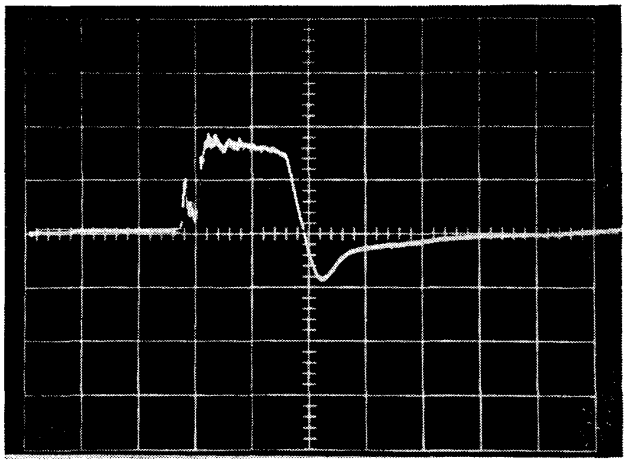

E−10−6

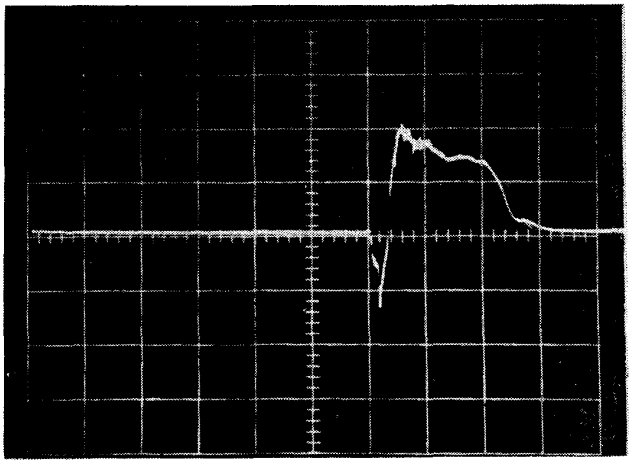

E−10−6
MPD only
without EBA fire.
MPD trigger pulse.

FIG. 3.6 (f). RPA data for EBA/MPD experiment
(V: 5V/Div. and H: 1 msec/Div.)

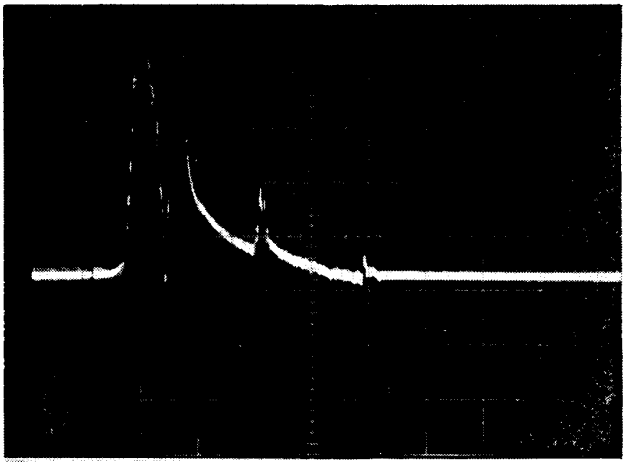

E−14−3
(EBA Only)

(V : 0.02V/Div
H : 10ms/Div)

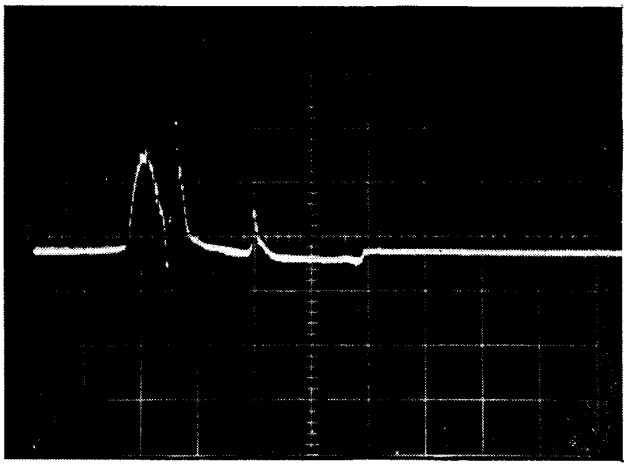

E−14−3a

(V : 0.05V/Div
H : 10ms/Div)

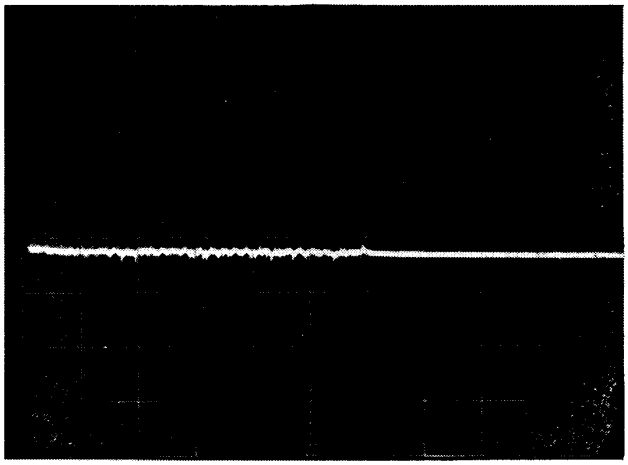

E−14−3b

(V : 0.05V/Div
H : 10ms/Div)

FIG. 3.7 (a). RPA data for EBA and EBA/NGP experiments.

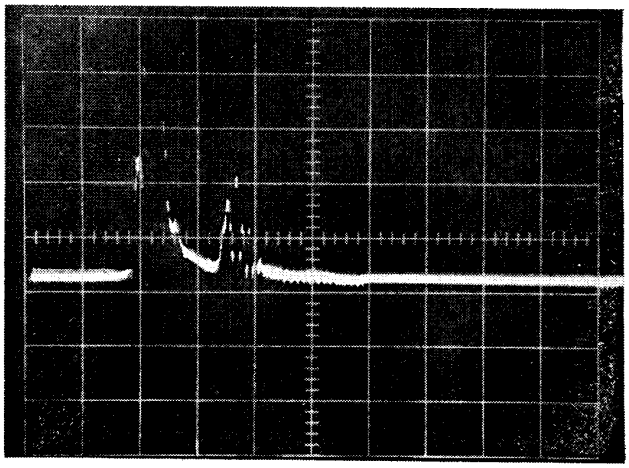

E−16−1a

(V : 0.02V/Div
H : 10ms/Div)

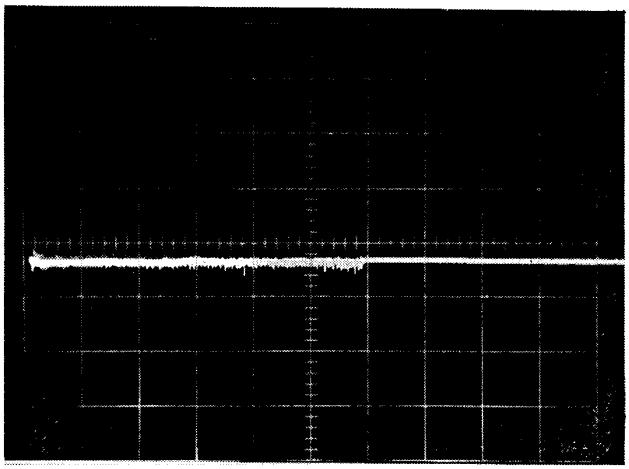

E−16−1b

(V : 0.05V/Div
H : 10ms/Div)

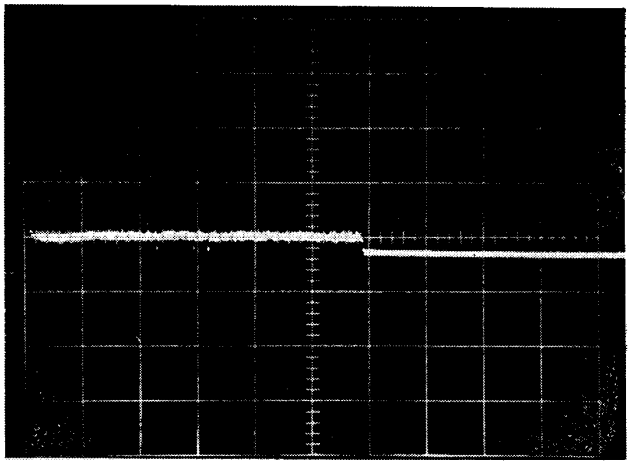

E−16−1c

(V : 0.05V/Div
H : 10ms/Div)

FIG. 3.7 (b). RPA data for EBA/NGP experiment.

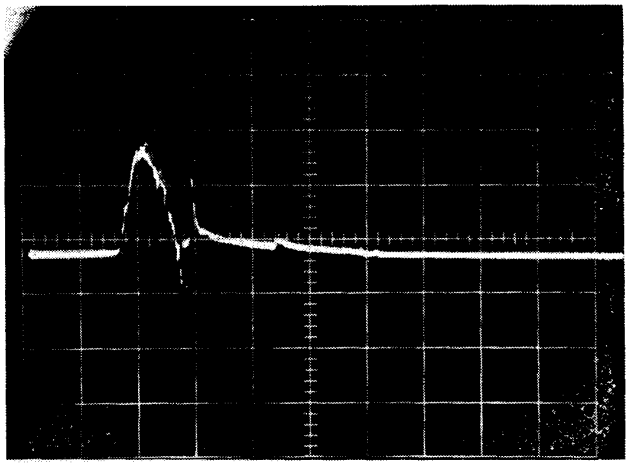

E−16−2a

(V : 0.05V/Div
H : 10ms/Div)

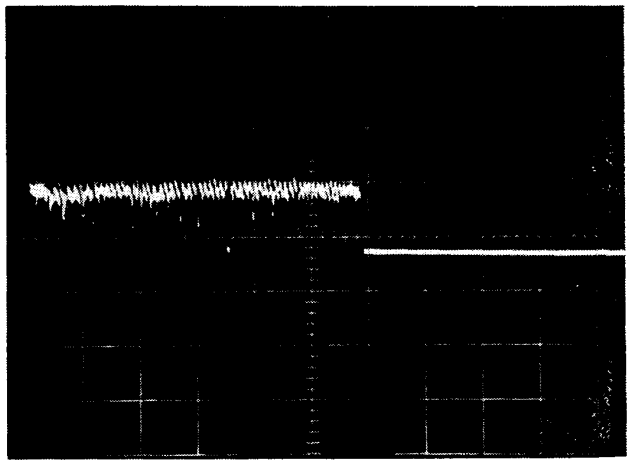

E−16−2c

(V : 0.05V/Div
H : 10ms/Div)

FIG. 3.7 (c). RPA data for EBA/NGP experiment

designed and fabricated to be the same as the PHO. Some comments on the results for comparing these two are given in sec. 7.

4.2 *PHO System*

The sensor consists of optical system and gimbal system. The optical system consists of a lens hood, an objective lens (100 mm diameter), three kinds of interference filters and one standard light source (fluorescent paint) for reference, 16 stages variable iris, and photomultiplier (multi-alkali photoelectric surface).

Two motors are used to change the filters and iris. Filters have 60% transparency with center wave lengths of 3914 Å, 5577 Å, and 6300 Å. The iris from 9° to null controls the incident light intensity, or changes a field view angle. Optical axis is changed by two-axis (2D) gimbal system to observe a light from any point in space along a beam.

The outside view of PHO is illustrated in Fig. 4.1. Coefficient to convert from the recorded output levels to input current to PHO pre-amplifier is 1μA/1V. The conversion from the output current of photo-multiplier to the incident light intensity has not calibrated yet but the relative intensity corresponding to each experiment condition can be analysed.

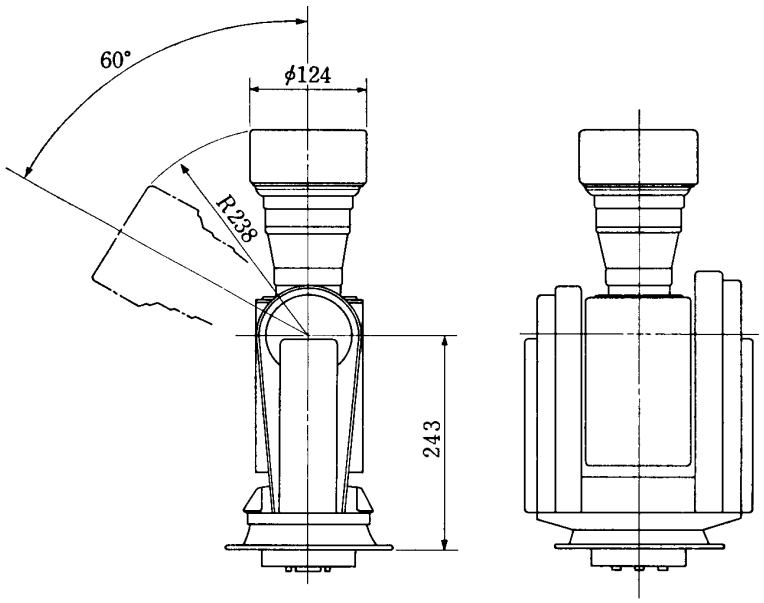

FIG. 4.1. Outview of PHO

4.3 *Experimental Results*

In this experiment, there are four kinds of accelerater operations i.e. MPD, EBA, EBA/MPD and EBA/NGP. Since the light intensity of a beam corresponding to EBA operation was very low compared to that of MPD plasma plume, the change in intensity of EBA beam due to simultaneous MPD operation is not clearly identified. To analyse the obtained data of PHO it should be noted that in this experiment configuration both EBA and MPD apertures faced towards top of the chamber where an aluminium cover reflect and scattered a light which may come into the PHO.

In the first day of the chamber pumping with liq. N_2, the temperature monitored in the PHO showed an extremely low temperature that indicated that the electrical heaters installed inside the PHO did not work properly. Since the control circuits to dirve motors were fortunately provided outside of the chamber, the over-driven currents were fed by refabricating a circuit. These data of temperature shall be introdued to design a flght model of PHO.

There are many irradiance profile measured corresponding various conditions mentioned in the Appendix. Here the typical one example for each operation mode are presented.

Fig. 4.2 illustrates PHO (3914 Å) and FP-TOP data for MPD (A–2 mode). In this figure 1.0 V of FP scale are equal to 500 V potential difference between FP-TOP probe and the FP ground. Scale of PHO indicate the output voltage of PHO pre-amplifier. The response of PHO system is reasonably considered to be less than 1 msec. The time delay of MPD light and FAVSCR is 1.2 msec. The decay time constant of the PHO output in this case shows a relatively very long time of an order of 10 msec, which has not yet been explained.

Fig. 4.3 depicts PHO (3914 Å) data for EBA (E–3–2 mode) operation. To

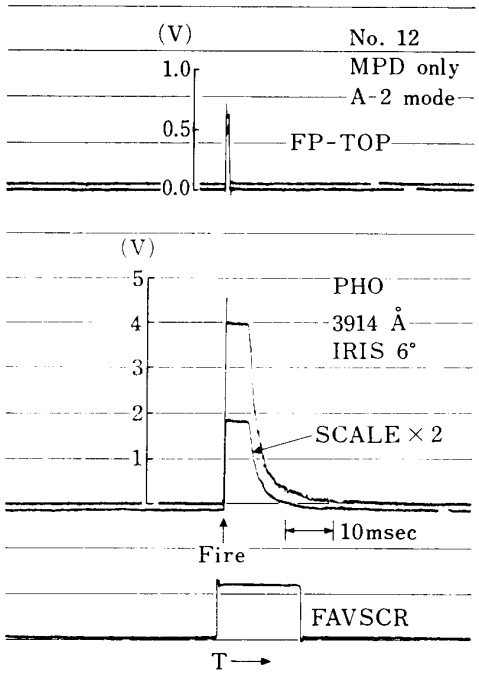

FIG. 4.2. PHO (3914 A) and FP-TOP data for MPD (A-2 mode).

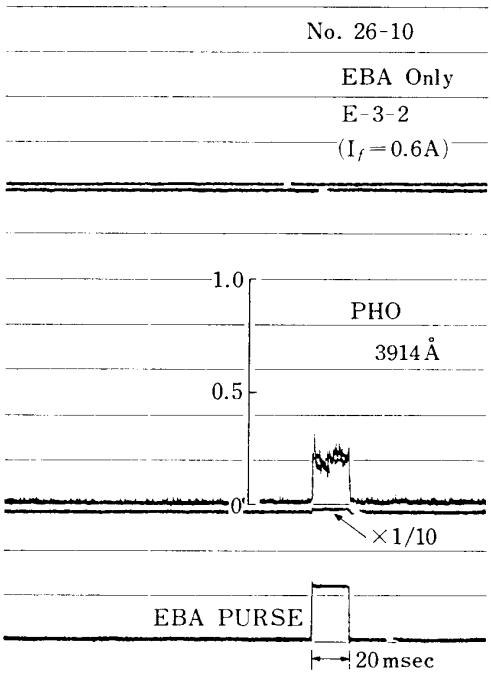

FIG. 4.3. PHO (3914 A) data for EBA (E-3-2).

compare with MPD data the level of light intensity is one order of magnitude low though the iris was fully opened. The fluctuation of light intensity is found to be very similar to the current fluctuation discussed in the previous section.

Figs. 4.4 and 4.5 are PHO (3914 Å) and FP data for the sumultaneous operations of EBA/MPD and EBA/NGP which are compared with a sigle operation.

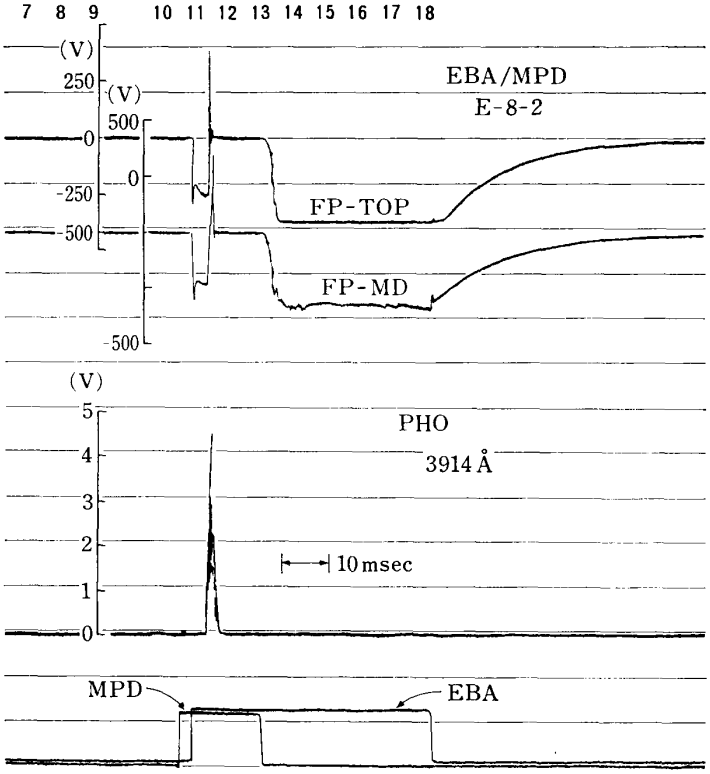

FIG. 4.4. PHO & FP data for EBA/MPD experiment.

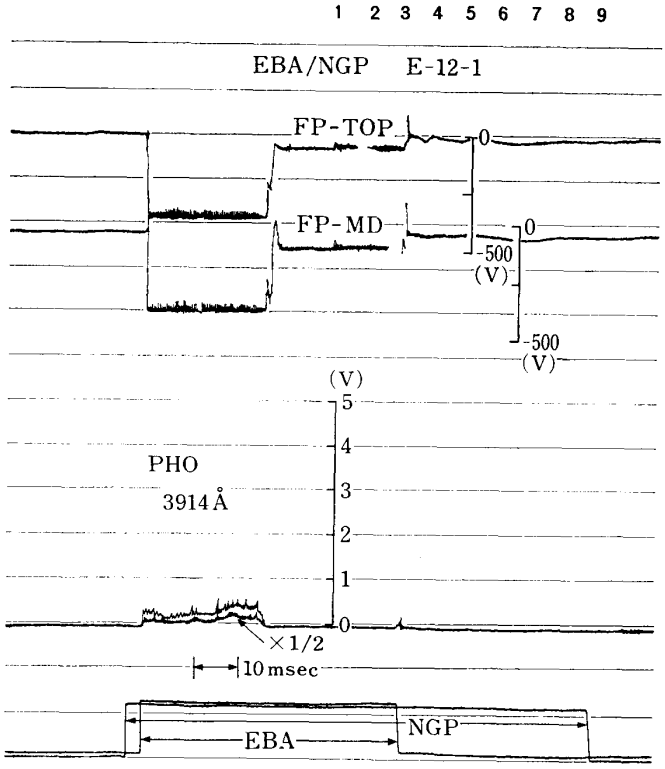

FIG. 4.5. PHO and FP data for EBA/NGP experimen.

4.4 *Conclusion*

PHO measured the irradiance due to beam-neutral gas interaction in the visible 3 kinds of wave length and check performance of an engineering model PHO to get technical data for the next flight model PHO design. The scientific discus sions here are insufficient and futher analysis is needed to improve the measurement.

5. PLP-FP Test

5.1 *General*

When an electron beam is emitted from Space Shuttle in the ionosphere, the vehicle electrostatic potential becomes positive with respect to the ambient plasma. The vehicle charging effect is one of very attractive themes in space plasma physics, and it is very important for the safety of the STS. In the SEPAC SL-1 experiment scheduled in 1981, an electron beam of 7.5 kV, 1.6 A (10 kW) will be emitted from the space shuttle to excite artifical aurora and plasma waves. The vehicle potential is to be measured by a floating probe system; the floating potential of the STS being estimated by measuring the voltage between the vehicle and a probe immersed in the ambient plasma. In this method, it is necessary to keep the probe outside of the plasma sheath of the vehicle. However, in the SL-1 experiment, the floating probe can not be extended outside the payload-bay envelope. The measured voltage between the vehicle and the probe does not always agree with the floating voltage of the vehicle with respect to the ambient plasma. Under such constraints, it is necessary to measure the spatial distribution of the potential by plural floating probes and to estimate the floating potential of the vehicle by extrapolating the distribution curve. The purpose of the present test is to verify that the floating potential of the vehicle can be measured by the floating probe system designed based on the principle mentioned above.

A floating probe system which is almost the same as used in the SEPAC SL-1 experiment was tested in the NASDA large chamber together with other SEPAC diagnostic instruments. Charging effect of the electron beam accelerator system due to beam emission and charge neutralization by a simultaneous ejection of MPD plasma or neutral gas plume (NGP) were successfully examined by the floating probe system.

5.2 *Floating Probe System*

The floating probe system used in this experiment consists of three spherical probes, 8 cm in diameter, arranged on an insulated pole with separation distance of 50 cm, as shown in Fig. 5.1. This system is set at about 3 m away from electrson beam accelerator. The whole experimental configuration is shown in Fig. 1.2. Each component except MTV has a common ground, which is isolated from the chamber wall. The common ground corresponds to the Shuttle ground in the SEPAC SL-1 experiment. Accordingly, the potential difference between the common ground and the chamber wall in this laboratory simulation corresponds to the floating voltage of the space shuttle with respect to the ambient

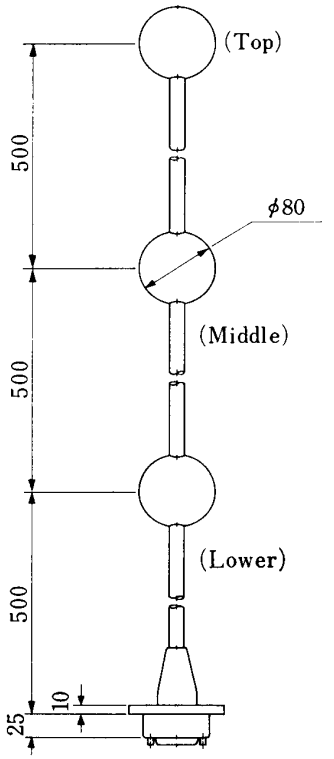

FIG. 5.1. The floating probe system.

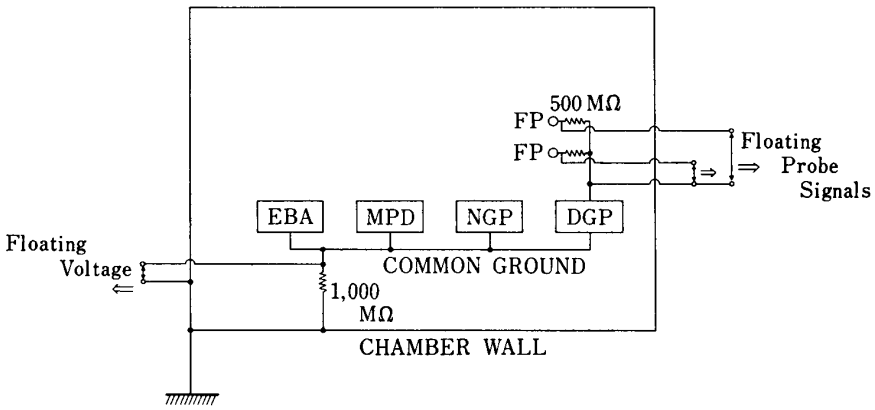

FIG. 5.2. Electrical relation between each component. The common ground is isolated from the chamber wall.

plasma outside the plasma sheath in space. This potential difference is measured directly by a high voltage probe and is compared with the two floating probe data. The electrical relation between each component and the chamber wall is illustrated in Fig. 5.2. The resistance from the probe to the floating common ground is 100 MΩ. The signal is divided by 2.5×10^3 in the pre-amplifier and is fed to detectors outside the chamber.

5.3 *Experimental Results*

A typical example of the floating probe voltage with respect to the common ground is shown in Fig. 5.3. The voltage between the floating common ground

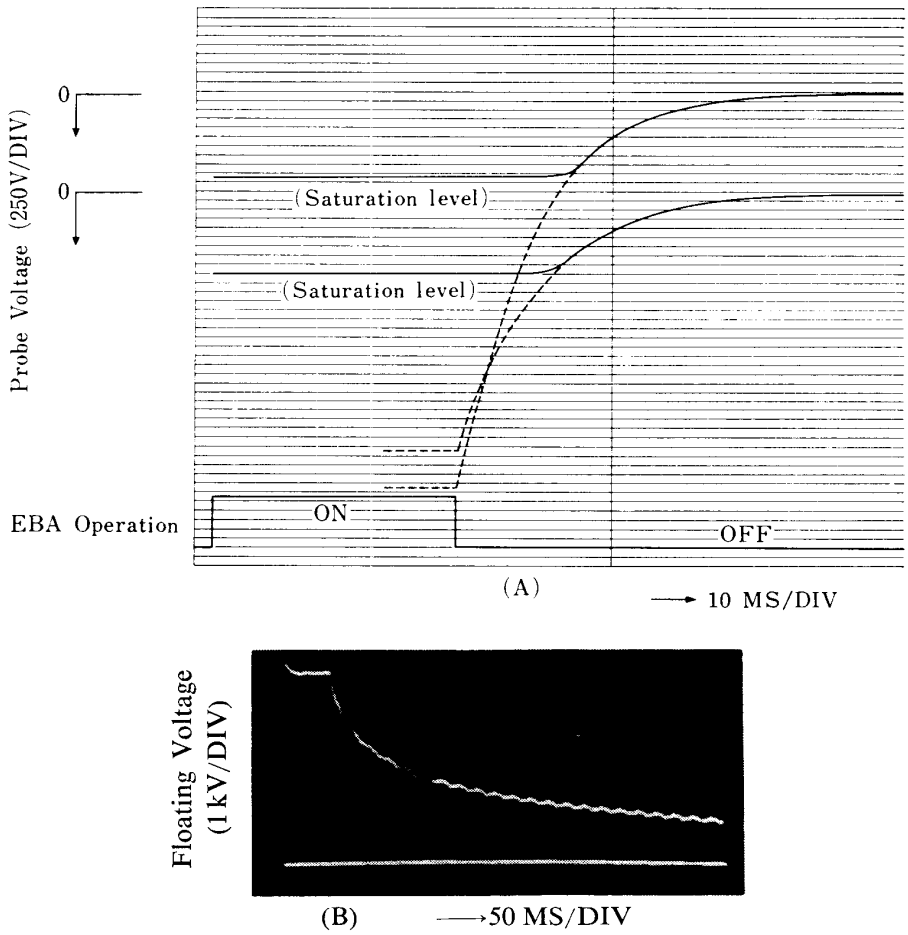

FIG. 5.3. (A) The time variation of the probe signals when an electron of of 5 kV 0.6 A is emitted. (B) The time variation of the floating voltage measured directly by a high voltage probe when an electron beam of 5 kV 0.05 A is emitted.

to the chamber wall is also shown for comparison. The upper trace corresponds to the signal measured by the top probe and the lower trace to that measured by the middle probe. Since the setting of the saturation level of the Pre-amplifier is too low, the signals are cripped at the saturation level. We can extrapolate the decaying curve to the real floating voltage as depicted by dashed lines in Fig. 5.3. The time-valiation of the signal responds to that of the floating voltage of the system with respect to the chamber wall which is directly measured outside the chamber, and the measured values reflect the spatial distribution of the potential. The voltage measured by the top probe is always larger than that measured by the middle probe. In high vacuum without plasma, the voltage between the probe and the common ground should not appear fundamentally, because the impedance between the probe and the chamber wall is much higher ($\sim$infinity) than that between the probe and the common ground. The voltage observed in this experiment is caused by the existence of rarefied plasma produced by the electron beam. The pressure inside the chamber is typically kept below 10^{-6} Torr. Though the background pressure is fairly low, the electron beam can still produce

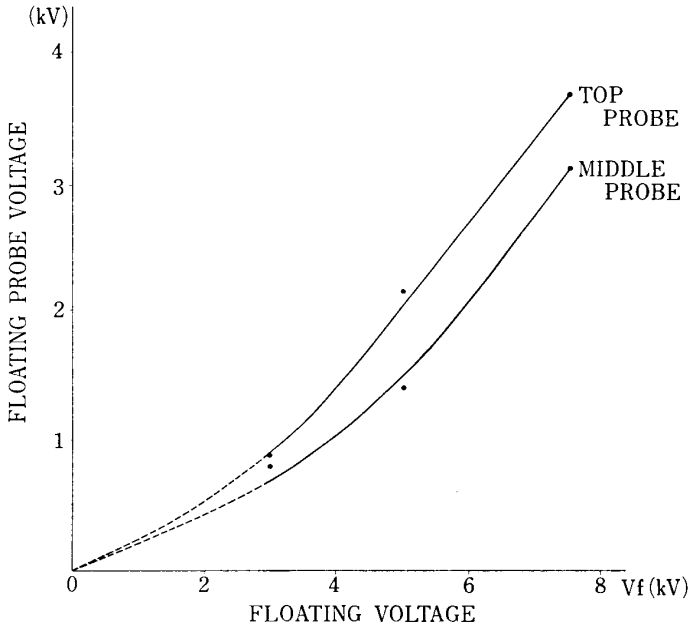

FIG. 5.4. The floating with respect to the floating voltage of the common ground with respet to the chamber wall.

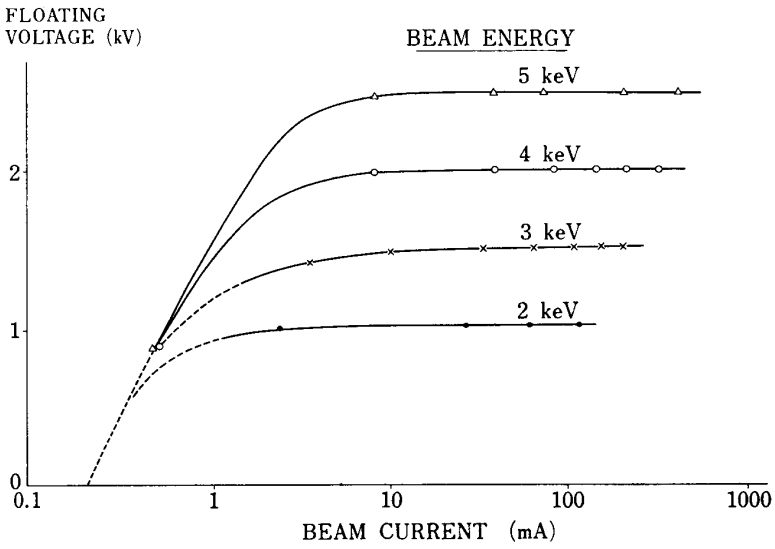

FIG. 5.5. The dependence of floating voltage on beam current.

a plasma of low density, which reduces the impedance between the probe and the chamber wall.

Fig. 5.4 shows the floating probe voltage with respect to the floating voltage of the common ground with respect to the wall. The voltage measured by the two probes reflects the floating voltage fairly well. The floating voltage between chamber wall and the grounding of EBA measured directly by a high voltage probe coincides with the beam acceleration voltage precisely when the beam current is large enough (Fig. 5.5). The data displayed in Fig. 5.4 are all obtained when beam current is larger than 100 mA.

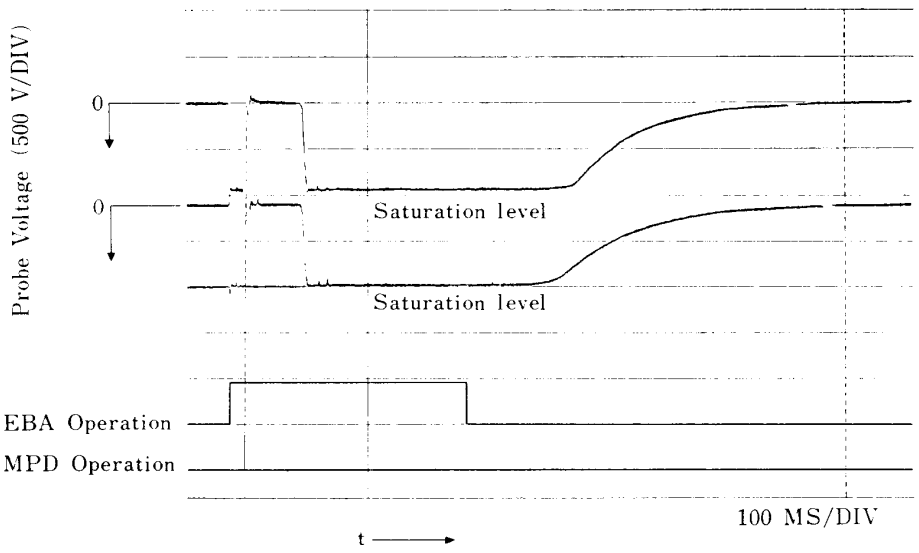

FIG. 5.6. Charge neutralization by a simultaneous ejection of MPD-AJ plasma. The signal of floating probes shows that the effect of neutralization sustains for a while after the termination of the plasma ejection.

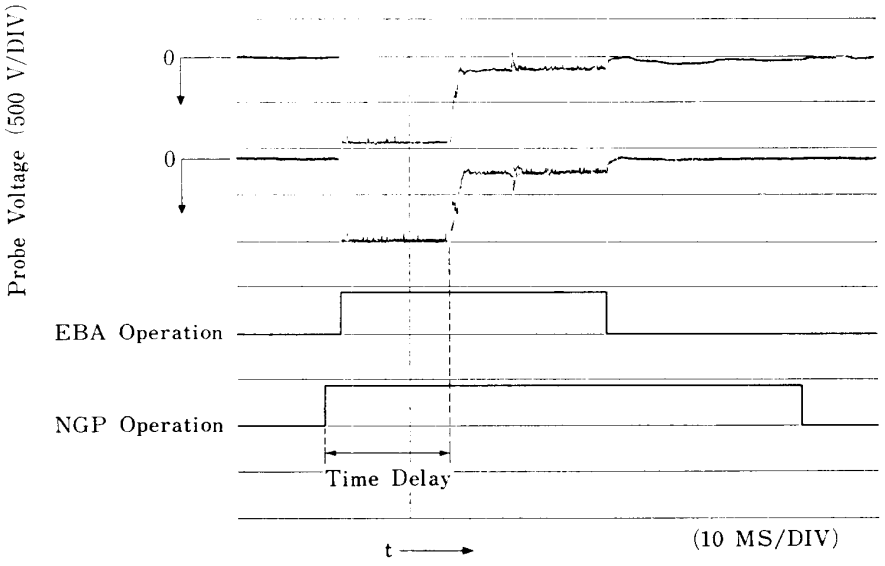

FIG. 5.7. Charge neutralization by a simultaneous ejection of neutral gas plume observed by the floating probes.

Since only two floating probes are used in the present experiment, it is impossible to estimate exactly the spatial distribution of the floating voltage. However, the fact that the potential variation can be measured by two probes located at different position suggests that the floating voltage of the Space Shutt will be estimated by using three probes at different position as designed for the SEPAC SL-1 experiment.

When the MPD-AJ plasma is injected during electron beam emission, the probe voltage vanishes abruptly (Fig. 5.6), corresponding to the decrease of the floating voltage which is due to decreased impedance between the common ground and the chamber wall by the MPD plasma. The same effect is also observed when

the neutral gas plume (NGP) is injected during beam emission, where neutral gas is ionized by the electron beam and plasma produced decreases the space impedance (Fig. 5.7). These are another evidence that the signal of the floating probe correctly reflects the floating voltage of the system.

5.4 *Conclusion*

The rise of the floating voltage of the electron beam accelerator system due to beam emission could be detected by the floating probe system in the NASDA large chamber experiment. It is found that the floating probe system is useful for measuring the floating voltage of the vehicle in the coming SEPAC SL-1 experiment. Further investigation is necessary to estimate the floating voltage of the vehicle.

6. PWP Test

6.1 *General*

PWP was designed to measure electromagnetic waves and electrostatic waves excited by EBA and/or MPD beams using several kinds of antennas (sensors). Since those waves have a wide range of frequency spectrum associated with dif--erent plasma resonance, cut-off and instabilities from a few tens of Hz to MHz, various techniques were developed, some of which would be used in SEPAC SL-1 experiment. Though it was difficult in this experiment to set a group of antennas

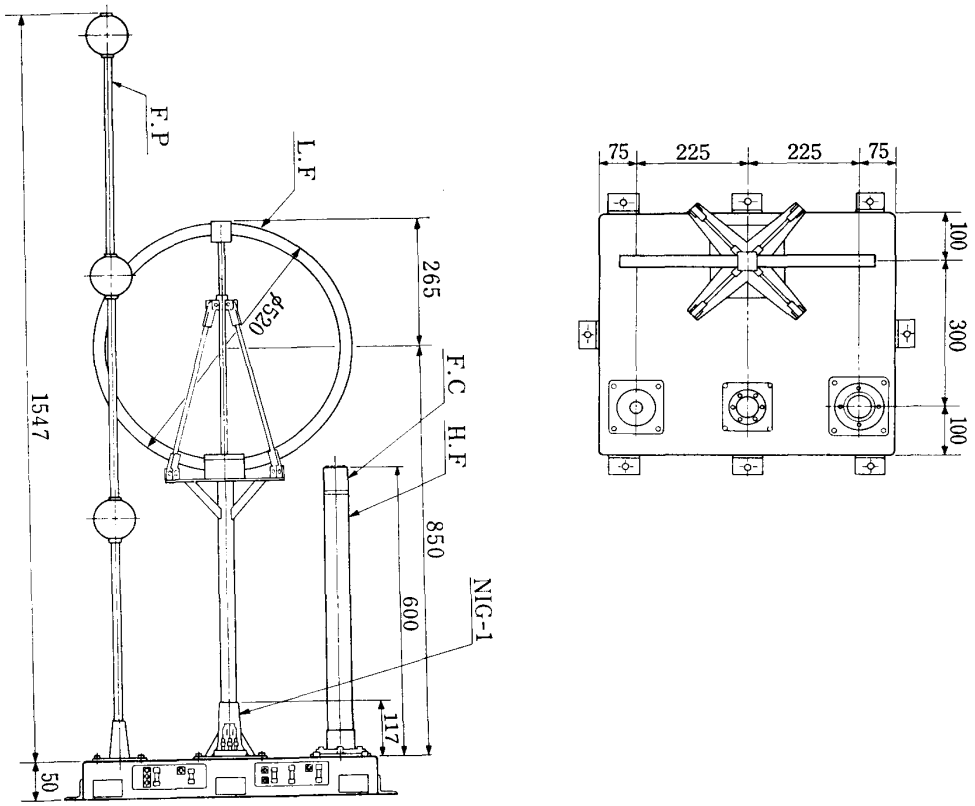

FIG. 6.1. DG antennas ; LF, FC, and HF are mounted together with FP and NIG-1.

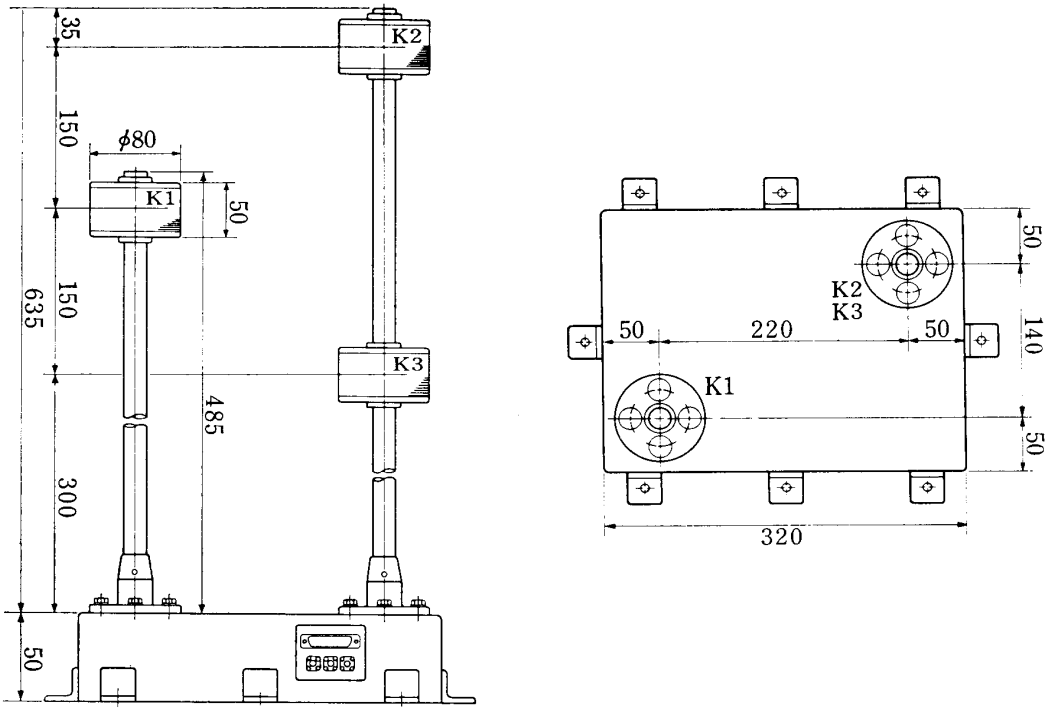

FIG. 6.2. DGP antennas; three K sensors.

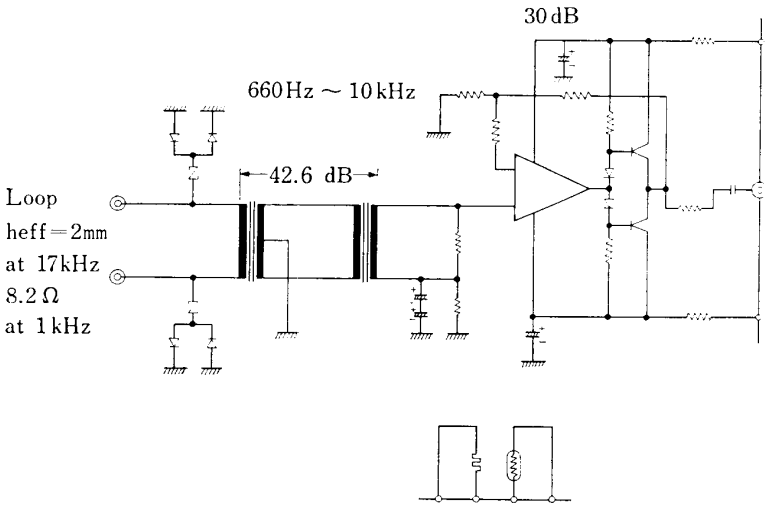

FIG. 6.3. Circuit diagram of Pre-amplifier of the Loop (LF).

at idealized places by or in or along a beam, the observed data give us many informations on the design of SEPAC/DGP-PWP as well as scientific data to examine characteristics of wave excitations by a beam in a vacuum chamber. These data are also correlated with other data measured by PHO, PLP, etc.

6.2 *Plasma Wave Probe system*

PWP system principally consists of several antennas (sensors) which detect magnetic/electric field and the recording system which records wide band data (VLF range) or field intensity data (HF range) through a spectrum analyser. Antenna system consists of a loop antenna (LF), a monopole (HF) and three

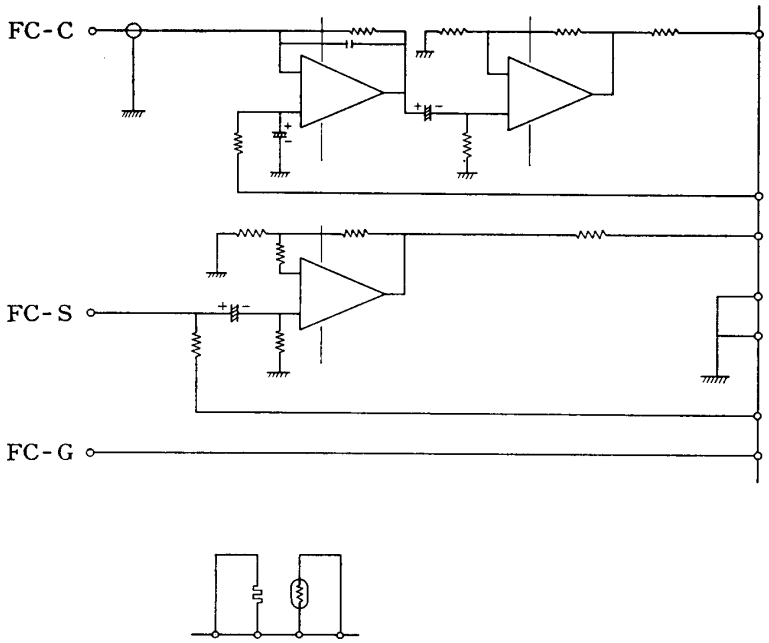

FIG. 6.4. Circuit diagram of Pre-amplifier of the FC.

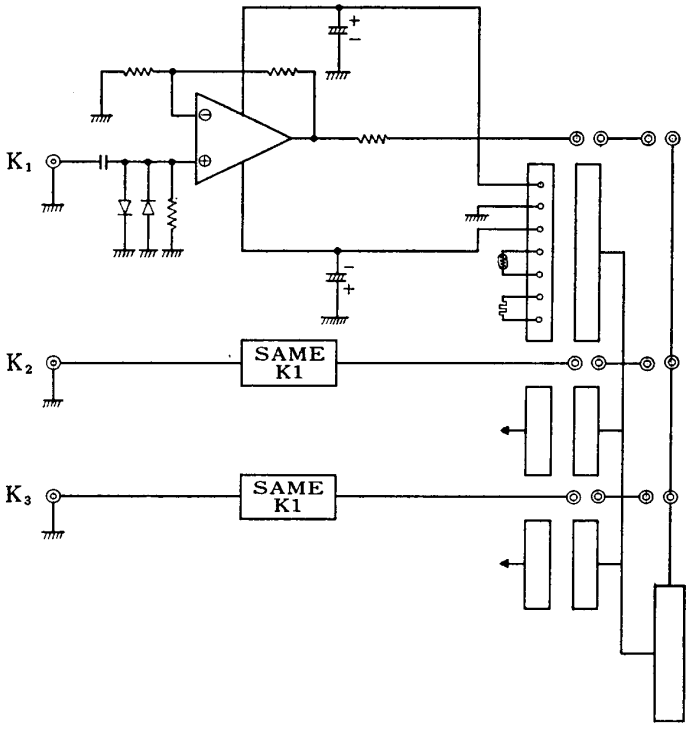

FIG. 6.5. Circuit diagram of Pre-amplifier of the K.

electric field pick-ups (K), and the Faraday Cup. The outviews of the system are depicted in Fig. 6.1 and 6.2 (see also Fig. 1.2 to check the antenna positions relative to the accelerators). LF (loop antenna), FC (Faraday Cup) and HF (a monopole) were mounted together with FP and NIG-1, and the other group is three K-sensors.

Figs. 6.3 to 6.5 are electrical circuit diagrams showing functions of preamplifiers

corresponding to each antenna. Since only qualitative discussions are given to the typical examples of output data which have been tentatively analysed, the characteristics of these circuits and recording instruments are omitted in this report.

6.3 *Experimental Results*

The typical examples are shown in Fig. 6.6. The upper panel is the data from

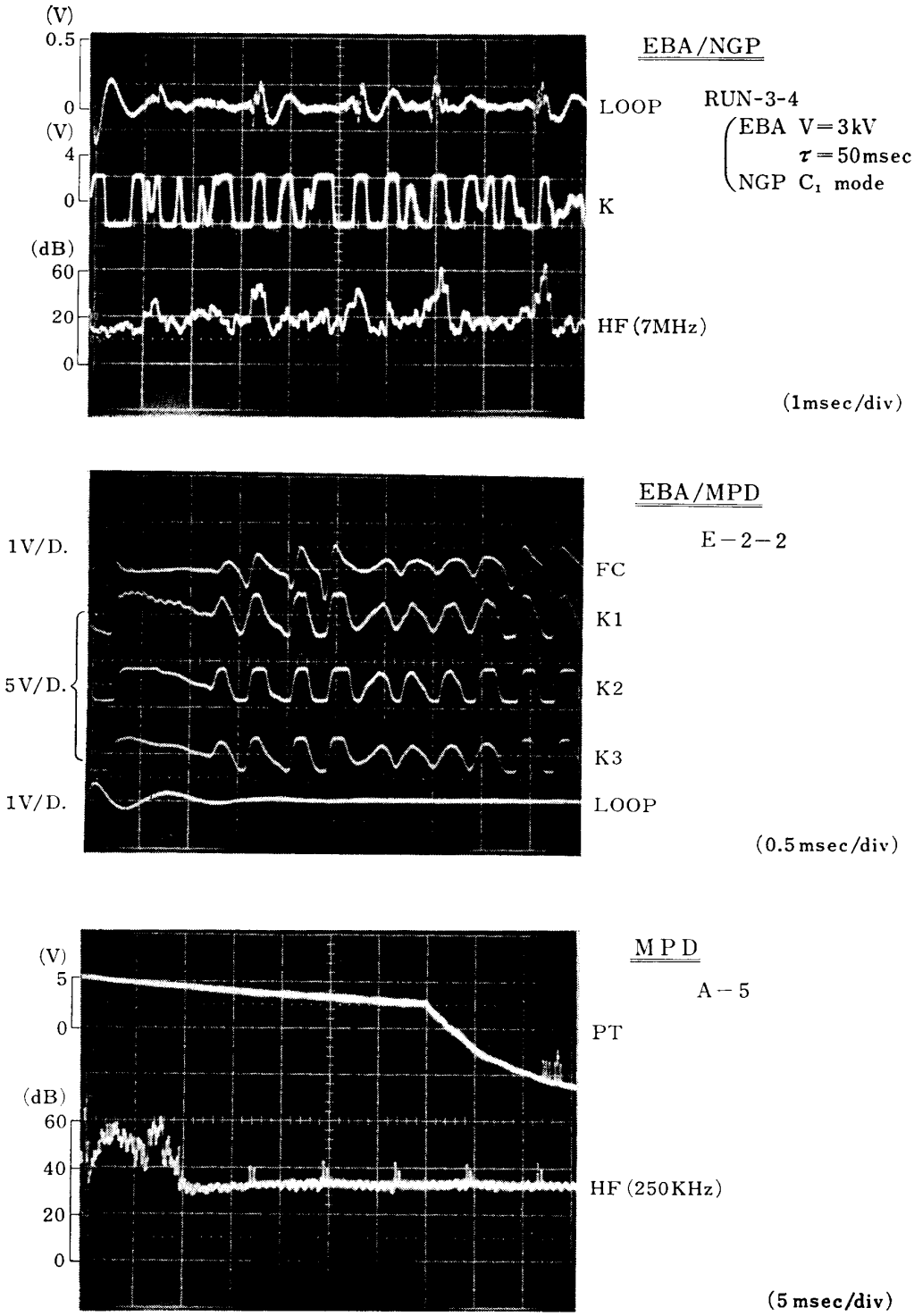

FIG. 6.6. PWP data

LF, K, and HF in the experiment RUN–3–4 (this is not included in Appendix) where EBA fired with 3 keV electron, time duration of 50 msec and NGP being simultaneously operated in C_1 mode. There is correlation between these three signals that the intensity of the loop signal increases accompanying with the increase of intensity of wide band signaf of K and the increase of 7 MHz intensity of HF. The fluctuation has a time scale of order of msec. The middle panel is the data from FC, K1$\sim$3, and LF in the experiment EBA/MPD E–2–2, which shows the changes of wave intensities at different locations being coherent. That means the wave length is much greater than a characteristic scale length of this system. The fluctuation of wide band intensity has a frequency of order of arround 2 kHz. The lower panel shows a behaviour of the potential of the metal surrounding a Faraday Cup (PT) in the experiment MPD A–5 mode. At the be ginning PT shows a saturation level, followed by a decay with a large time constant giving no wave data. HF shows a wave excitation together with plasma beam emission.

6.4 *Conclusion*

Above is only one example to show how PWP instruments were performed in the chamber test, but ample of data were recorded corresponding to all operational mode cited in the Appendix. Further quantitative data analysis and their theoretical interpretations will be carried out not only in order to improve a SEPAC/DG–PWP instrument and its operation, but also to investigate a beam instability in this kind of experiments.

7. MTV Test

7.1 *General*

The MTV is to monitor the operation of the SEPAC particle accelerators and to observe a light emmision phenomena by the particle beams in the vicinity of the shuttle and in the earth's atmosphere.

In this chamber test, the engineering model of MTV was placed at one corner of the platform where all SEPAC test equipments were installed. Several engineering data were taken to study the characteristics in the vacuum environment surrounded by the wall with a very low temperature due to the cooling shrouds (liq. N_2). EBA electron beams and MPD plasma plumes were monitored on the TV screen by this MTV.

7.2 *Monitor TV system*

The MTV is a low light monocro TV camera consisting of F 25 mm auto-iris lens and silicon-intensifier target (SIT) camera tube. The viewing axis is determined by vertical and horizontal motions of two-axis gimbal. The whole camera system is contained in an air-tight cannister (vessel), a dry nitrozen gas being filled in it.

The electrical characteristics are:

a. Type NTSC, Monocro 525 lines 60 field 2:1 interlace

b.	Aspect Ratio	4:3
c.	Image Tube	RCA 4804, spectrum response 390 nm–700 nm
d.	S/N Ratio	40 dB p–p/rms
e.	light control range	0.01–10^5 lux
f.	lens	Focal length 25 mm F 0.81
		FOV 28.7°×21.7°, Fixed focus
g.	Video Bandwidth	4.5 MHz
h.	Video Signal	EIA-std, RS–170
i.	Frame Rate	30 Hz
j.	Line Rate	15.75 kHz

Above data are useful to interpret the observed picture of a beam, because, for example, the time correlation between MTV line scanning and beam emission profile must be taken into account in this experiment.

Fig. 7.1 is a picture to show the MTV in the chamber (see also Fig. 1.2).

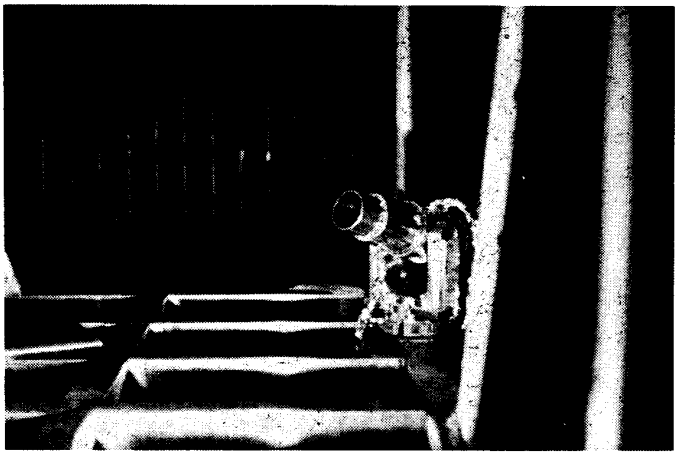

FIG. 7.1. MTV Engineering Model in the chamber.

7.3 *Expermental Results*

The MTV successfully monitored all operations performed inside a chamber throughout this test. The pictures showing an electron beam pass corresponding toeach EBA operation in Fig. 3.1.2 of Report No. 562 are copies of MTV picture monitor. Another picture to monitor MPD plasma plume ejection taken by this MTV is already shown in Fig. 3.2.2 of Report No. 562. Though the analysis of these pictures have not been done yet, all recorded data tapes are available to look at the accelerater operations.

In this experiment, there are several problem similar to that of PHO. The light reflected from the aluminum cover and other construction materials reduced the S/N ratio of a TV picture.

7.4 *Conclusion*

The engineering model MTV was tested and data for design of MTV PM/FM systems and for operations of SEPAC/MTV are now available. The thermal data analysis in this test has been done and the results give a guidline for thermal

design of MTV. The pictures of EBA/MPD beams suggest some ideas to construct MTV–GSE (Ground Support Equipments) for post-mission data analyses which, of course, are very useful for data recording and analysis systems for MTV AT/QT (Acceptant Test/Qualification Test) etc.

8. ISAS Test Participants

The member of ISAS team participated in this experiment is listed below.

◦ General Test Conductor	T. Obayashi
◦ Test Manager	K. Kuriki
◦ Electron Beam Accelerator	
Manager	N. Kawashima
Member	S. Sasaki
	A. Yamori
	TOSHIBA Elec. Co.
◦ MPD Arcjet/Neutral Gas Plume	
Manager	K. Kuriki
Member	K. Nakamaru
	Y. Shimizu
	T. Araki
	MITSUBISHI Elec. Co.
	MEISEI Elec. Co.
	MITSUBISHI Heavy Ind.
◦ Diagnostics	
Manager	M. Ejiri
Member	S. Miyatake
	MEISEI Elec. Co.
	TOSHIBA Elec. Co.
◦ EMI Test	
Manager	I. Kudo
Member	MITSUBISHI Elec. Co.
◦ Mechanical Structure	
Manager	T. Araki
Member	K. Kuriki
	USHIO Elec. Co.
	YUSHIYA Man. Co.
◦ Safety	
Manager (Mechanical)	T. Araki
Manager (Electrical)	N. Kawashima

Department of Space Science
Institute of Space and Aeronautical Science
University of Tokyo
May 24, 1978

I. MPD-AL (MELCO)

ID	DLYT	FAVP	CHGV 1
A1	1.2 ms	2 AT	480 V
A2			400
A3			350
A4			300
A5		1 AT	400
A6			350
A7			300

DLYT: Delay time
FAVP: Fast Acting Value Pressure
CHGV 1: Charger Voltage

II. MPD-AJ (MEC)

ID	DLYT	FAVP	CHGV 1
B1	0.8 ms	1.5 AT	480 V
B2			400
B3			350
B4			300
B5		1 AT	400
B6			350
B7			300
B8	1.2 ms	1.5 AT	480
B9			400
B10			350

III. NGP

ID	EJNP	EJNT
C_1	3.6 AT	0.1 s
C_2		0.2
C_3		0.5
C_4		1.0

EJNP: Ejection Pressure
EJNT: Ejection Time Duration

IV. EBA

ID	V (kV)	I_H (A)	I_B (mA)	τ (ms)	F/E*
E-1-1	1.3	13	700	50	E
2	2				
3	4				
4	6				
5	7.5				
E-2-1	1.3	14			
2	2				
3	4				
4	6				
5	7.5				
E-3-1a	1.3		400	50	
b			500		
c			600		
d			700		
e			800		
f			900		
g			1000		
h			1100		
2a	2.0		400		
b			600		
c			800		
d			1000		
3a	4.0		500		
b			700		
c			900		
d			1000		

*{ F: Floating mode
E: Earth mode

I_B: Beam Current
τ: emission duration time
I_H: Heart Current

V. EBA/MPD

ID	V (kV)	I_H (A)	I_B (mA)	τ (ms)	F/E	MPD
E-7-1	1.3	14	40	50	F	A_1
2			90			
E-8-1	3		45			
2			270			
E-9-1	5		3			
2			10			
3			30			
4			100			
5			300			
6			400			
E-10-1	5		400			A_1
2						A_2
3						A_3
4						A_4
5						A_1
6						A_3
E-11-1	7.5		900			A_1

VI. EBA/NGP

ID	V (kV)	I_H (A)	I_B (mA)	τ (ms)	τNE(S)	F/E	NGP
E-12-1	6	14	500	50	0	F	C_1
2					0.5		
3					1.0		
4					1.5		
5					1.25		
6					1.75		
7					2.0		
E-14-1a	5		4		0		
b					0.5		
c					1.5		
2a			40		0		
b					0.5		
c					1.5		
3a			400		0		
b					0.5		
c					1.5		
E-16-1a	2		110		0		
b					0.5		
c					1.5		
2a	5				0		
b					0.5		
c					1.5		

τNE(s): time delay of EBA firing from NGP ejection (sec).